# *THE LUMINOSITY FUNCTION OF GALAXIES IN THE COMA CLUSTER AND IN ITS OUTSKIRTS*

---

*Bachelor of Science Thesis*

*By*

Eftychia Madika [1]

*Thesis Supervisor:*

Prof. Manolis Plionis

[1] *Physics Department, Aristotle University of Thessaloniki, Thessaloniki Greece 54124*

May, 2015

This page intentionally left blank.

# Abstract

In this thesis we estimate the Schechter luminosity function (LF) of different types of galaxies in the rich Coma cluster, in order to search for environmental affects. We use the SDSS DR10 spectroscopic galaxy catalogue. Initially we select as cluster members those that meet certain criteria, and then we correct the magnitudes, in the three bands g, r and i , for systematic effects. We study the shape of the galaxy LF within a radius of $R = 1.5h_{72}^{-1}$ Mpc, for the whole sample of galaxies and separately for the ellipticals, spirals and irregulars. To this end we apply for the estimation of the LF's parameters the $\chi^2$ minimization procedure. The elliptical galaxies dominate the form of the LF due to the fact that they are more numerous. Subsequently, we study the shape of the LF in the dense core of the cluster, which is dominated by ellipticals, and in the less dense outskirts, where the number density of the spirals is relativity higher. Finally we study the dependence of the LF's parameters $\alpha$ and $M^*$ on the radial distance from the cluster center.

# Περίληψη

Στην εργασία αυτή υπολογίζουμε την συνάρτηση φωτεινότητας των γαλαξιών που ανήκουν στο πλούσιο σμήνος γαλαξιών, Coma. Το δείγμα των γαλαξιών είναι από το φασματοσκοπικό κατάλογο γαλαξιών του SDSS DR10. Θεωρώντας την συναρτησιακή μορφή Schechter της συνάρτησης φωτεινότητας, υπολογίζουμε τις παραμέτρους α και M* χρησιμοποιώντας όλους τους γαλαξιές που εμπίπτουν στα κριτήρια να είναι μέλη του σμήνους. Εν συνεχεία υπολογίζουμε τις παραμέτρους της συνάρτησης φωτεινότητας ξεχωριστά για τους ελλειπτικούς, σπειροειδείς και ανώμαλους γαλαξίες και στα τρία φίλτρα g , r και i. Παρατηρούμε ότι η επίδραση των ελλειπτικών γαλαξιών στην συνολική μορφή της συνάρτησης ειναι πολύ μεγάλη καθώς ειναι κυρίαρχοι στο σμήνος. Έπειτα μελετάμε τη μορφή της συνάρτησης Schechter στον πυρήνα του σμήνους, ο οποίος έχει μεγάλη αριθμητική πυκνότητα και κυριαρχείται κυρίως από ελλειπτικούς γαλαξίες, και στις παρυφές του σμήνους, όπου η πυκνότητα ειναι πολύ μικρή ενώ το ποσοστό των σπειροειδών γαλαξιών ειναι αρκετά μεγάλο. Τέλος, μελετάμε την εξάρτηση των παραμέτρων της συνάρτησης λαμπρότητας από την απόσταση από το κέντρο του σμήνους, ώστε να κατανοήσουμε την επίδραση του εγγύς περιβάλλοντος στα ποσοστά των διαφορετικών ειδών γαλαξιών αλλά και στη συνάρτηση φωτεινότητας του.

# Acknowledgements

I would like to express my gratitude to my supervisor, Prof. Plionis Manolis for guiding, motivating, encouraging and helping me throughout this thesis. I would also like to thank my family for the constant support and assistance. Finally, a very special thanks goes out to my boyfriend and fellow student Konstantinos Nikolaos Migkas for his patience, daily support and invaluable help.

# Contents

# 1 Introduction

The effort of understanding the Universe as a single entity may have been the most ancient question of all, even if the ideas and tools that people used throughout the years were not necessarily scientific. Observational Cosmology attempt to study the evolution of the Universe and its large scale structure as well as to fully discover all of the Universe's contents, through observations. It has radically developed since the middle of the $20^{th}$ century with its most important achievements being the discovery of the Cosmic Microwave Background (CMB), the discovery of Dark Matter, the surveys of the millions of galaxies and thousands of galaxy clusters and of course the accelerated expansion of the Universe which revealed the necessity of the so-called Dark Energy.

## 1.1 Cosmological model

The current generally accepted cosmological model depends strongly on the Cosmological Principle, which states that the Universe is isotropic and homogeneous for scales larger than 100 Mpc. In other words, the Hubble expansion is a function only of redshift $z$ and not of the direction on the sky. Moreover, except for regular baryonic matter, there is the Cold Dark Matter, to which we attribute nearly the 25% of the total mass-energy density of the Universe, while the absolute dominant substance is the Dark Energy which represents approximately the 70% of the total mass-energy density. Trough the Friedman's equation, the Hubble parameter $H(z)$ is given by:

$$H(z) = H_0 \sqrt{\Omega_{m,0}(1+z)^3 + \Omega_{k,0}(1+z)^2 + \Omega_\Lambda \exp\left(3\int_0^z \frac{1+w(x)}{1+x}\,\mathrm{d}x\right)} \tag{1.1}$$

where $\Omega_{m,k,\Lambda}$ are the normalised, present epoch, density parameters for the matter (baryonic + Dark), the curvature and the Dark Energy respectively, while $H_0$[1] is the Hubble constant. The different cosmological parameters affect the luminosity distance of a celestial object for a specific $z$. In this thesis the cosmological parameters do not play a major

[1] $Ho = 72h_{72}\ km/s/Mpc$

role in our analysis and therefore we use the most recent and widely accepted values, which are those for a $\Lambda$CDM model.

We can calculate the luminosity distance $d_L$ of an astrophysical object for a flat geometry Universe as follows:

$$d_L = c(1+z)\int_0^z \frac{\mathrm{d}x}{H(x)} \tag{1.2}$$

This quantity is related to the apparent and absolute magnitudes $m$ and $M$ of a light source (galaxies in our case) through the distance modulus equation:

$$\mu = m - M = 5\log d_L + 25 \tag{1.3}$$

There are also other factors that interfere with our measured apparent magnitudes that we will analyse in the next chapter.

## 1.2 Structure formation theory

The Cosmic Microwave Background (CMB) reveals an impressive amount of homogeneity between different sky regions. However, there are temperature fluctuations of the order of $10^{-5}$. These temperature fluctuations also reflect density fluctuations of the same order in the early Universe that would eventually grow and become galaxies and galaxy clusters.

In the early Universe there were quantum fluctuations in the matter-energy density that became larger and macroscopic as the size of the Universe increased. The generally accepted mechanism through which this happened is the inflation, during which the Universe expanded rapidly for about $10^{-32}$ $s$ causing the existing quantum perturbations to increase dramatically. Therefore, there were regions, of radius $r$, with higher matter density $\rho(r)$ than the average $\overline{\rho}$, described by the quantity:

$$\delta(r) \equiv \frac{\delta\rho}{\overline{\rho}} = \frac{\rho(r) - \overline{\rho}}{\overline{\rho}} \tag{1.4}$$

The subsequent formation of the large scale structure of the Universe is a result of gravitational instability of these fluctuations. When a region is overdensed ($\delta(r) > 0$), the matter contracts because of the attracting forces and as a result $\delta$ increases. Of course, there are factors that resist this gravitational collapse, such as pressure effects and the Hubble expansion. These two factors act as a "friction" term. This can cause the matter of a region not to collapse if the force of gravity cannot surmount the resisting forces. The starting phase of a possible gravitational collapse can be well described in the framework of linear growth of structure which is provide by the linear perturbation theory (eq. Wintraecken, 2009). The time evolution equation of which is:

$$\ddot{\delta}_k + 2H\dot{\delta}_k - 4\pi G\overline{\rho}\delta_k \left[1 - \frac{\pi u_s^2}{\lambda^2 G\overline{\rho}}\right] = 0 \tag{1.5}$$

where $\delta_k$ the transformation of $\delta$ in the Fourier space, $G$ the universal gravitational constant, $u_s$ is the speed of sound $\left(u_s = \sqrt{\dfrac{\partial p}{\partial \rho}}\right)$ and $\lambda = \dfrac{2\pi\alpha}{k}$, with k the wave number. As we can see from eq. (1.5) if the quantity in the brackets of the last term is positive, the gravity overcomes the "friction" term and therefore the perturbations can grow larger. This means that for that to happen the length scale $\lambda$ must be:

$$\lambda > \lambda_J = u_s \left(\frac{\pi}{G\overline{\rho}}\right)^{1/2} \tag{1.6}$$

where $\lambda_J$ the Jeans length, the crucial length scale that determines the evolution of small-scale irregularities in an expanding Universe. The most common definition for it, is the length scale for which the two opposing forces balance. The second term of eq. (1.5), known as the "Hubble drag" is produced by the cosmic expansion and acts as a resisting force to the gravitational collapse as we mentioned before.

If gravitational collapse was a result only of the existence of baryonic, "regular" matter, the current age of the Universe would not be enough for the large scale structure to form. Right after the recombination, the Universe can be described accurately by an Einstein-de Sitter model (a model with only matter and no Dark Energy or curvature) since the mass-energy density of baryonic+Dark matter is much greater than this of Dark Energy. Also, since matter has an equation-of-state parameter $w = 0$ it has no pressure, and the sound velocity $u_s$ in eq. (1.5) becomes $u_s = 0$, the pressure term vanish. Taking all these into account, it can easily be proven that today's value of the perturbations are related to those at the recombination epoch by:

$$\delta_0 = \delta_{rec}(1 + z_{rec}) \tag{1.7}$$

where $z_{rec} \approx 1100$ is the redshift in the recombination epoch and $\delta_{rec} \sim 10^{-5}$ the perturbations in the matter distribution then, as we stated before. Thus, in the present epoch the perturbations should be $\delta_0 \sim 10^{-2}$. Instead, the bulges of galaxy centres usually have densities a million times larger than the average density of the Universe which is $\overline{\rho} \approx 1.88 \times 10^{-29} gr/cm^3$. This means that there are structures with $\delta_0 \approx 10^6$. So, the cosmological models with only baryonic matter are not able to produce this kind of structure within the current age of the Universe (13.8 billion years). In order to explain such large amplitude perturbations we need Dark Matter, which due to its abundant existence, and the fact that it interacts only through gravity with the baryonic matter starts its gravitational collapse much earlier than the recombination.

In this case, the average density parameter in eq. (1.5) is the sum of the Dark Matter and the baryon density parameters, $\overline{\rho} = \overline{\rho}_{DM} + \overline{\rho}_b$. Since $\overline{\rho}_{DM} \gg \overline{\rho}_b$ and assuming that the Universe can be described by an Einstein-de Sitter model until the first $\sim 6$ billion years, it can be proven for the perturbations of baryonic and Dark Matter that they are related to the scale factor as displayed:

$$\delta_b \simeq \ \delta_{DM} \left(1 - \frac{\alpha_{rec}}{\alpha}\right) \tag{1.8}$$

Eq. (1.8) shows that for $\alpha \gg \alpha_{rec}$ (in the first 500 million years after the Big Bang is $\alpha \approx 100 \cdot \alpha_{rec}$) we see that $\delta_b \simeq \delta_{DM}$. Knowing that Dark Matter is far more dominand than the baryonic one and that it has no radiation pressure, it starts collapse gravitationally much earlier than the baryonic matter. As a result we can have structures forming in the first hundred million years of the Universe.

There are two main forms of Dark Matter that have been studied in the past, Hot (HDM) and Cold (CDM). Each type depends on the mass of the particles that it consists of. HDM consists of low-mass neutral particles that at the epoch of decoupling they were (ultra)relativistic. The best example of such particles are the neutrinos. For instance, while the decoupling time of neutrinos is $t \sim 1\ s$ at a temperature $kT \sim 1\ MeV$, a neutrino with rest energy of $m_v c^2 < 2\ eV$ would be relativistic even a little after the radiation-matter equality ($t_{eq} \sim 50000\ yr$) (Ryden 2007).

To find out the expected structure that results from HDM models we have to take into account that the expansion of the Universe caused the initially relativistic particles to lose energy and cool. Though, they remained relativistic until their thermal velocities were significantly lower than $c$ when $kT \sim m_v c^2$ (Bond, Efstathiou & Silk 1980). This corresponds to the equality temperature, $T_{eq} \sim 11600 \cdot m_v\ K$ and to an age of the Universe of $t_{eq} \sim 1.7 \times 10^{12}\ (m_v)^{-2}$ s. Thus, before this epoch, neutrinos and other possible relativistic HDM particles, move freely in random directions. This so-called "free streaming" motion tends to erase density fluctuations smaller than $\sim ct_{eq}$. This corresponds to a physical scale of $\lambda_{eq} \sim 18(m_v)^{-2}\ kpc$ or a comoving length scale of $L_{eq} \sim 60/m_v\ Mpc$. If we assume that at the present epoch is $\Omega_{m,0} = 0.3$ then the mass that corresponds to a sphere of radius Ł$_{eq}$ is $M \sim 10^{16}\ M_{\odot}$, which is a typical mass for superclusters. Therefore, the larger structures, such as superclusters, should had been formed earlier than the smaller scale structures. This scenario is called the "top-bottom" scenario. Clusters of galaxies, galaxies and stars are supposed to be a result of the fragmentation of "superclusters-like" systems. This scenario is not capable of explaining very old systems of small scales such as quasars and early galaxies. In addition, observations show that superclusters are not gravitationally bound yet, so the HDM model is not supported by the data and has been abandoned since the 80s .

On the other hand, CDM consists of high-mass, nonrelativistic at their decoupling epoch, particles. A very small fraction of CDM is represented by MACHOs (MAssive Compact Halo Objects), which consist of normal baryonic matter that may emit very faint or no radiation. Possible examples of MACHOs are black holes, neutron stars, brown dwarfs or Jupiter like planets. The main candidates for CDM are the WIMPs (Weakly Interacting Massive Particles) and the axions. WIMPs usually are considered to have rest energies $m_w c^2 \in [1\ GeV, 1\ TeV]$ and their free streaming is insignificant in cosmological terms.

Considering their behaviour, for a WIMP with $m_w c^2 \sim 1\ GeV$ its equality temperature ($kT \sim m_w c^2$) is $T_{eq} \sim 10^9\ K$ and the corresponding time is $t \sim 5\ s$. At this epoch the Hubble distance is $c/H(t) \sim 2ct \sim 2 \times 10^9\ m$[1] and the comoving length scale is $L_{eq} \sim 0.05\ kpc$. Therefore, the mass that is included in a sphere with radius $L_{eq}$ for $\Omega_{m,0} = 0.3$ is $M \ll M_{\odot}$, 18 orders of magnitude lower than the corresponding value for HDM. As a result, the fluctuations in matter are more intense in smaller scales and the first things that form due to the gravitational instability are globular cluster size objects then galaxies and finally superclusters. This scenario, in which smaller structures are formed first is called the "bottom-up" scenario. This agrees with the observed structure of the Universe since galaxies are the oldest systems, while cluster of galaxies are formed subsequently and superclusters are still in the process of collapsing. The conclusion is that CDM is the the most successful Dark Matter model to date.

[1]For the radiation epoch ($t = 5\ s$) the Hubble parameter is given by $H(t) = \frac{1}{2t}$

## 1.3 Large scale structure

The observable large scale structure is the result of the gravitational collapse of baryonic matter within the gravitational field, mainly of Dark Matter, as we analysed above. The main cosmic structures are galaxies, clusters of galaxies, superclusters, filaments and voids.

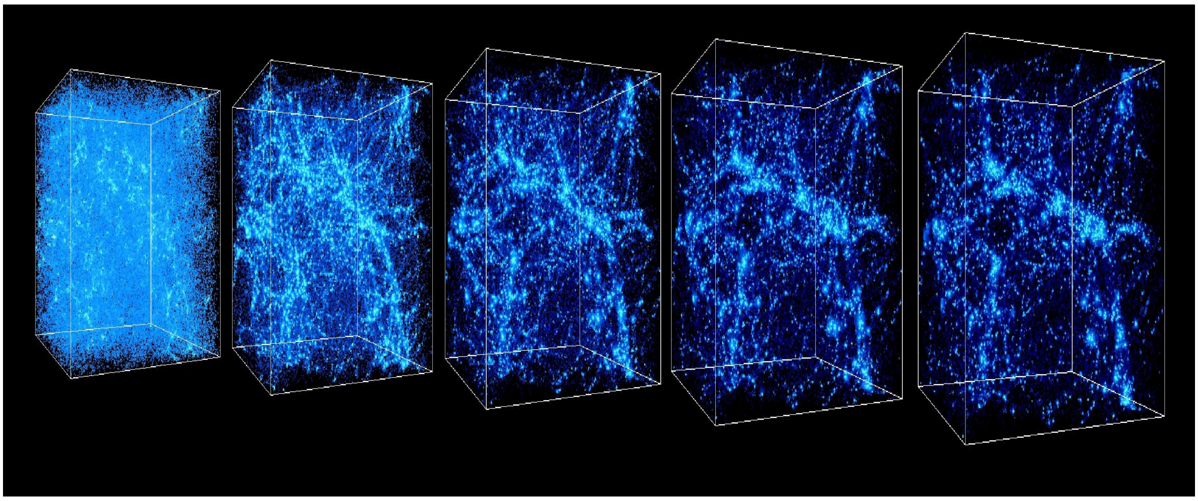

**Figure 1:** Simulation of how the large scale structure evolves with time, from the early Universe (left) to today (right)

### 1.3.1 Galaxies

The basic unit of collapsed matter in the Universe are the galaxies. Galaxies are probably the earliest large-scale structures to form due to gravitational instabilitity. They consist of stars, gas, dust and Dark Matter with proportions that differ between galaxies and which are strongly depended on galaxy type. Their star-number can vary between a few hundred of thousands of stars to one trillion, while their typical diameters are from a few kpc's to some hundreds of kpc's. Most of them contain a central supermassive black hole. The different types of galaxies were initially categorised by Hubble in 1926. In his famous "tuning-fork" diagram the position of a galaxy is determined by its shape, by the size of its nucleus and the spiral arm tilt. The three main categories are the ellipticals ($\sim$ 15% of all the observed galaxies) which for historical reason are referred to as "early types", the spirals ($\sim$ 60%) or "late types", the irregulars ($\sim$ 5%) and the lenticulars (or SO's, $\sim 20\%$). The oldest galaxies that have ever been observed are over 13.1 billion years old, so they were formed in less than 800 million years after the Big Bang.

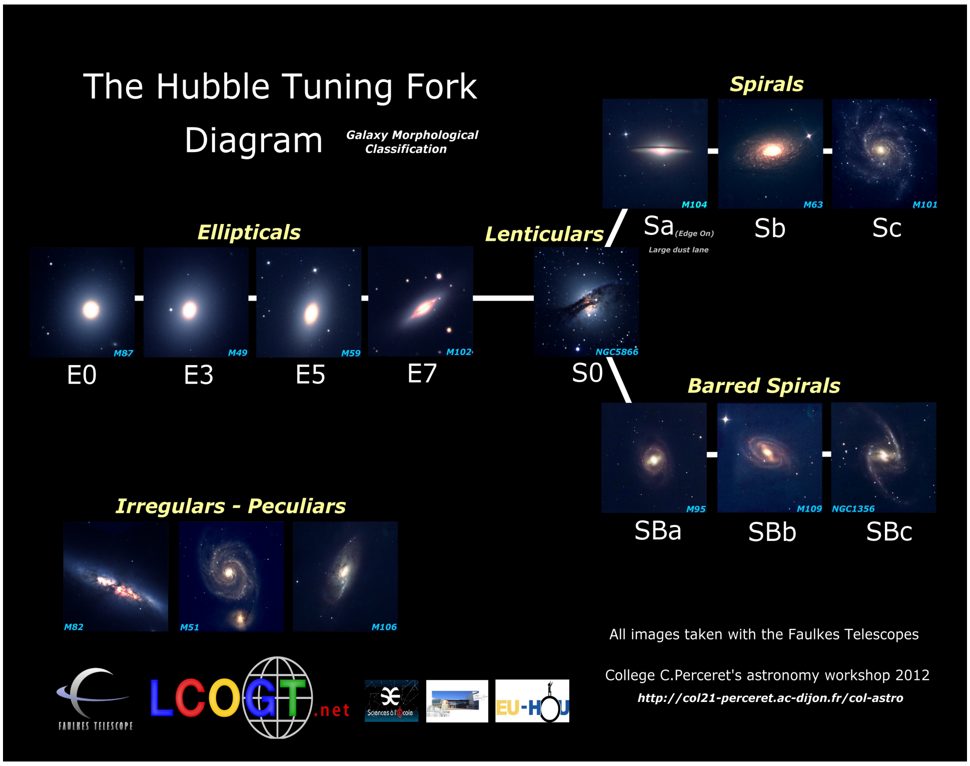


**Figure 2:** The Hubble's "tuning-fork" diagram for galaxy categorization.

Spiral galaxies consist of three parts, the disc, the bulge and the halo. Their main characteristics are a flat rotating disc, which has a thickness of only a few hundreds of pc's and their bright spiral arms in which intense star formation takes place due to the large amount of gas and dust that they contain. Their blue color indicates the rich young O and B star population. The bulge usually contains older stars with low metal content, with a number density of 1000 stars/pc$^3$, 4 orders of magnitude greater than the spiral arms stellar density. Moreover, the whole galaxy is surrounded by many globular star clusters and old stars, located in the halo of the galaxy. The mass of spiral galaxies varies from $10^8\ h^{-1}\ M_{\odot}$ to $10^{12}\ h^{-1}\ M_{\odot}$. Their mass-to-light ratio has a range $\frac{M}{L} \sim (2-20)h$.

Elliptical galaxies are ellipsoidal systems that contain old stars and very little cold gas and dust, therefore there is almost none star formation. On the contrary, they contain significant amounts of hot X-ray emitting interstellar gas that can not collapse gravitationally. The most massive and luminous galaxies, observed in the Universe, are ellipticals since they can reach a mass of even $10^{13}\ h^{-1}\ M_{\odot}$. On the other hand, there are dwarf ellipticals with $10^{7}\ h^{-1}\ M_{\odot}$, a little larger than typical globular star clusters. Their brightest stars are red giants and supergiants. They are considered to be the oldest galaxies that firstly formed and to have this shape due to the important velocity dispersion of their stars. Their mass-to-light ratio usually is $\frac{M}{L} \sim (20-100)h$.

### 1.3.2 Galaxy clusters

Galaxy clusters are cosmic laboratories that can be used as very useful tools for extragalactic astrophysics and helping us to study the components and physical properties of the large scale structure of the Universe. They form at the intersections of the sheets and filaments of the large scale structure as it is analysed below. Currently, they are thought to form via hierarchical clustering, a process by which smaller structures (galaxies in this case) merge due to gravity to form larger structures. As they grow, they accrete more mass from the filaments within which they are embedded (Jones et al. 2010). They are the largest gravitationally bound systems in existence and a large fraction of them are dynamically relaxed. Their centres are dominated by elliptical galaxies, while spirals are mostly located in their outskirts (Dressler et al. 1997). This is due to the fact that (giant) ellipticals are older than spirals and they had enough time to in-fall into the cluster's potential while spirals are younger and they are usually not into full dynamical equilibrium within the cluster (they are still in-falling). There are also other explanations why ellipticals are far more common near the centre of clusters, as we mention below. The two youngest clusters that have ever observed are the ClG J02182-05102 at $z = 1.63$ ($\approx$ 9.6 Gyr old) (Papovich et al. 2010) and the JKCS 041 at $z = 1.8$ ($\approx$ 10 Gyr old) (Andreon et al. 2009; Newman et al. 2014). Nearly half of galaxies in the Universe are within clusters.

The smallest clusters of galaxies contain some tens of galaxies while the most massive ones have some thousands of members and have typical diameters inthe range of one to a few Mpc. Clusters with less than 20 galaxies are called "galaxy groups" (Mulchaey 2000) and have typical mass $M \sim 10^{13} h^{-1}\ M_{\odot}$. These astrophysical systems were first studied at the beginning of the $20^{th}$ century and in 1933 F. Zwicky made an estimation of the Coma cluster's mass. He found that there was a need for a significant amount of mass which was unobserved and which later called Dark Matter. Nowadays we know that $\sim 85\%$ of the mass of clusters is in the form of Dark Matter, while the typical masses of clusters are in the range $M \sim 10^{13} - 10^{15} h^{-1}\ M_{\odot}$. They contain significant amounts of hot ionized X-ray emitting gas that makes them visible even at very large redshifts. In addition, diffuse radio emission has also been detected in galaxy clusters (Ferrari et al. 2008).

There are several ways to categorize clusters the most common of which is between regular and irregular clusters. Both categories can be further divided into two subcategories, rich clusters ($\geq 50$ members) and poor clusters ($< 50$ members).

*Regulars* are characterised by their smooth and spherical symmetric structure, their small proportion of spiral galaxies ($\leq 20\%$) which are located mainly in their outskirts, their highly dense centre with $\geq 10^3\ Galaxies/\mathrm{Mpc}^3$ (Bahcall 1996) and their high X-ray luminosity due to the large amounts of hot gas. Most of them contain $\geq 1000$ galaxies. Moreover, their velocity dispersion is high and of the order of $\sim 10^3\ km/s$, something that together with their smooth structure is considered to be the result of the fact that they are relaxed, in virial equilibrium. Thereby, subclustering is not significant in this type of clusters. Finally, there are more massive than other cluster types while in the center we usually observe one or more giant elliptical galaxies. Coma cluster is such a regular cluster.

*Irregulars* are identified by their lumpy structure which has no symmetry, their high fraction of spirals ($\geq 40\%$) and their lower X-ray luminosity. Additionally, due to their low velocity dispersion sometimes substructures of double or multiple systems of galaxies are present in these clusters (Forman et al. 2002). There is no easily distinguished centre while the number of galaxies is $\leq 1000$. Finally, their mass is usually an order of magnitude lower than the mass of the regulars clusters. A well-known irregular cluster is the Virgo cluster.

Another noteworthy category of clusters is those which have a central large bright galaxy,

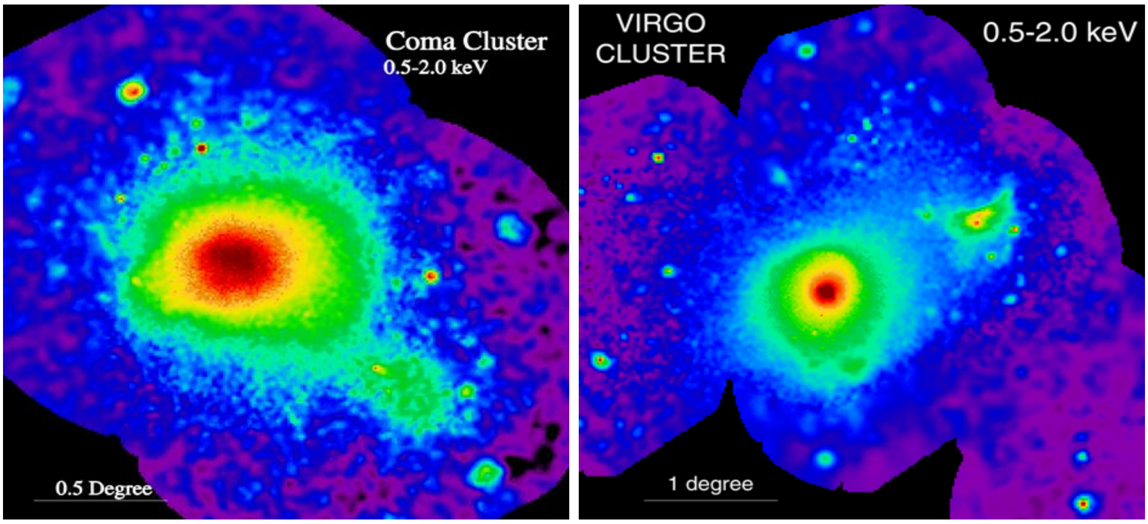


**Figure 3:** *Left panel:* The regular Coma cluster in X-rays. *Right panel:* The irregular Virgo cluster in X-rays.

called BCG (Brightest Cluster Galaxy) or cD galaxy (supergiant diffused ellipticals). These huge galaxies have a mass of $M \geq 10^{12}\ h^{-1}\ M_{\odot}$ and can have more than one nuclei. A generally accepted scenario for their formation is that of "galactic cannibalism" which refers to the process of the collision of two or more galaxies due to tidal gravitational interactions that leads to the merger of these galaxies and the formation of supergiant elliptical galaxy. Another common scenario claims that these huge galaxies might have been formed in special locations which happen to be the cores around which clusters formed via anisotropic accretion of mass (West 1994).

A different categorisation of galaxy clusters is that of Bautz & Morgan (1970) and it separates clusters into five classes. In the first class belong clusters which at their centres have dominant supermassive cD galaxies that emit significantly in the optical wavelengths. The fifth class does not contain galaxies that are distinguishable from the other normal bright galaxies of the cluster. The intermediate classes have central galaxies with descending luminosity from the first to the last class.

Another important characteristic of galaxy clusters are the so-called morphology-density relation (MDR) and a lot of studies have focused in it. Firstly, Dressler (1980) showed, using 55 rich clusters, that the higher the density of a cluster, the higher the fraction of elliptical and SO galaxies and, correspondingly, the lower the fraction of spirals. This outcome is independent of the type of the cluster. Moreover, Van der Wel et al. (2007) confirmed the above result and also studied the evolution of the early-type galaxy fraction with redshift both for the field as well as for within groups and clusters. It was showed that for galaxies with masses $M \geq 4 \times 10^{10}\ h^{-1}\ M_{\odot}$ the fraction does not change significantly with time, being $48 \pm 7\%$ for $z \sim 0.8$ and $43 \pm 3\%$ for $z \sim 0.03$. This means that the MDR does not change significantly with redshift. This result has a key role in understanding the effect that the environment dependencies of galaxy evolution. However, systematic uncertainties of the morphology is a possibility since it is relatively difficult to distinguish ellipticals or S0's from face-on spirals, although such spirals are not that common.

### 1.3.3 Superclusters, filaments and voids

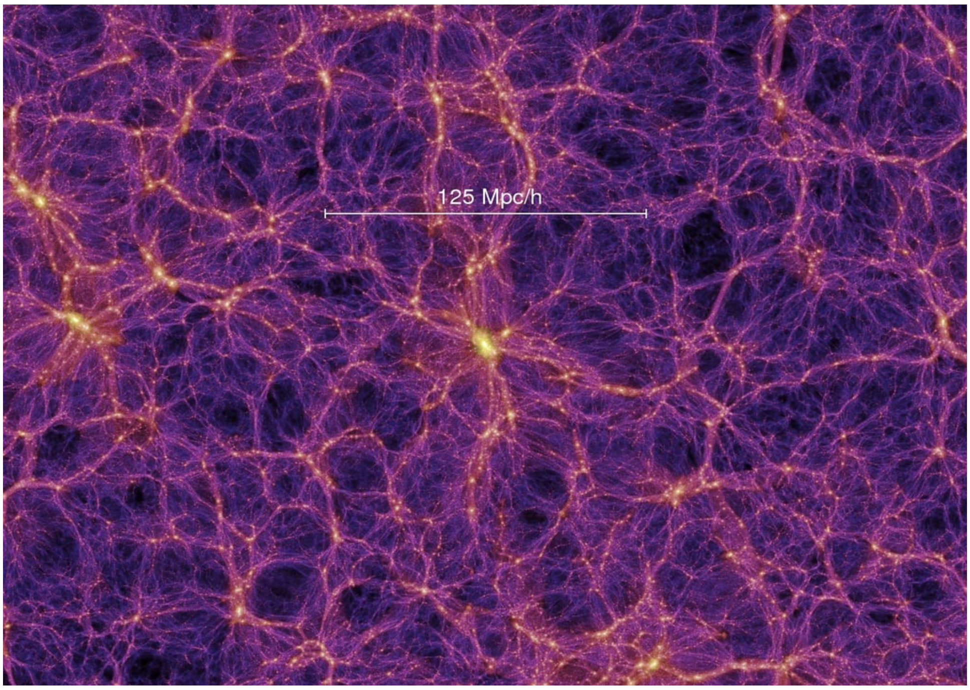


**Figure 4:** Simulation of Superclusters, filaments and voids

*Superclusters* are groups of galaxy clusters and galaxy groups. Generally, they are defined as groups of two or more galaxy clusters above a given spatial density enhancement (Bahcall 1988). They are the only larger in size isolated systems than galaxy clusters but they are not gravitationally bound since they haven't have enough time to collapse under their own gravity within the age of the Universe. This results from the fact that a typical cluster's peculiar velocity is $\sim 10^3$ km/s and thus the distance that it could move within a Hubble time it is $10h^{-1}$ $Mpc$ while the typical size of a supercluster is $30-50h^{-1}$ Mpc. However, their size can reach even $\sim 150h^{-1}$ Mpc as seen in some filamentary structures (Chon et al. 2014). Usually their appearance is generally not spherically symmetric but rather irregular, usually flattened and elongated.

*Filaments* are long bridges of gravitationally bound galaxies that connect rich clusters and usually they constitute the boundaries of large voids. Their typical size is $\sim 40-60h^{-1}$ Mpc. Using simulations, Aragón-Calvo et al. (2010) showed that filaments contain 40% of the total mass content of the current Universe while they occupy only 10% of space. Most evolutionary structure formation models claim that these structure get tighter with time but not longer.

*Voids* are large semi-spherical regions with no luminous galaxies and with very low average density surrounded by filaments and sheets of galaxies(van de Weygaert & Platen 2011). Their typical size is $15h^{-1}$ Mpc and their mean overdensity factor $\delta$ as defined by eq. (1.4) is $\delta \approx -0.94$ (Coil 2012). The lack of luminous matter probably provides an ideal place to test different galaxy formation models, according to Peebles (2001).

## 1.4 Luminosity Function

One of the most basic tools in the study of galaxy clusters is the galaxy luminosity function (hereafter LF) of their members. LF gives the expected number (density) of galaxies $\Phi(L)dL$ within a luminosity interval $[L, L + dL]$ over an appropriately defined volume (Spinrad 2005) and provides the luminosity and absolute magnitude distribution of galaxies within the clusters or groups of galaxies or even the field. In 1976, P. Schechter published the most common and efficient expression of the LF for galaxy clusters so far (Schechter 1976) which is:

$$\Phi(L)dL = \frac{\phi^*}{L^*}\left(\frac{L}{L^*}\right)^{\alpha} \exp\left(-\frac{L}{L^*}\right)dL \tag{1.9}$$

which, if we combine it with

$$M^* - M = 2.5 \log \frac{L}{L^*}$$

we get the Schechter LF in terms of absolute magnitude, so

$$\Phi(M)dM = 0.4 \ln 10 \ \phi^* [10^{-0.4(M-M^*)}]^{(1+\alpha)} \exp{[-10^{-0.4(M-M^*)}]} dM \tag{1.10}$$

where $\phi^*$ is a normalisation factor (number per volume, $Mpc^{-3}$), $M^*$ is the characteristic absolute magnitude at which the LF change significantly from the exponential law to the power law (it represents the "bend") or in other words the luminosity where the brighter galaxies are separated by the fainter ones. Finally, $\alpha$ is the slope of the LF in the faint-end, when $M > M^*$. Most light of a cluster comes from galaxies with $M \approx M^*$ since the brighter ones are relatively rare and the fainter ones are too faint (Hansen et al. 2005).

The Schechter LF has many advantages such as being analytic, continuous and having many mathematical properties. Generally, the main reasons we want to study the LFs of galaxies within clusters and to constrain their parameters are that, firstly, we want to compare their LFs to that of the field galaxies. Doing this, we will be able to understand the importance and influence that environment has on the evolution and population of galaxies (Popesso et al. 2005). Furthermore, we can compare different galaxy clusters and find out if approximately the same parameters' values describe similar clusters or the luminosity distribution is strongly depended on each cluster, something that could indicate differences in the processes of cluster formation. Also, valuable information is provided by the LF regarding the formation of new galaxies, the primordial density fluctuations that gave birth to the cluster as well as the transformation processes of mass into light.

Montero-Darta & Prada (2009) used the 516,891 galaxies in r-band contained in the SDSS DR6 release and calculated the Schechter LF parameters as follows: $\alpha = -1.23 \pm 0.02$, $M^* = -20.73 + 5\log h \pm 0.04$ and $\phi^* = (0.9 \pm 0.07)h^3 \times 10^{-2}\ Mpc^{-3}$. For these values, we can calculate the mean luminosity density using eq. (1.9) as following:

$$\langle L \rangle = \int L\Phi(L)dL \approx 2 \times 10^8 h\ L_\odot\ Mpc^{-3} \tag{1.11}$$

Through several studies some characteristics concerning the shape of the LF for different galaxy types or for different environments have been observed. To begin with, all giant types of galaxies (Ellipticals, Irregulars and Spirals) have a maximum in their luminosity function while Irregulars and Spirals appear to a Gaussian distribution of luminosities. Additionally, for a single Hubble type of galaxies, the LF does not change significantly for regions with high or low density. Therefore, the parameters in the Schechter LF does not significant changes between different galaxy types but apparently not between different environments so it is very important to study these differences and to extract conclusions about the magnitude characteristics for different Hubble types (Wen & Han 2014), but also to check for possible environmental dependencies.

# 2 Observational Data

Clusters of galaxies are important tools of extragalactic astrophysics, for studying the formation, the evolution and the interactions between the galaxies in cluster environments. The form of the galaxy LF in the cluster core region and in the outskirts, where the number density of galaxies is different, leads to an estimation of the cluster's regions properties. In addition, the extraction of the LF for elliptical, spiral and irregular galaxies separately, gives essential informations in terms of attributes of different kind of galaxies.

## 2.1 The cluster sample and its basic properties

In order to perform an investigation of the shape of the LF in different bands (g, r, i), we chose one of the biggest clusters from the Abell (1958, ACO 1989) cluster catalogue, the A1656, known as Coma Cluster. The A1656 is one of the richest clusters at low redshifts ($z = 0.0231$), having a luminosity distance of $D_L = 97.9\ Mpc$ and equatorial coordinates $\alpha = 194.95^o$ and $\delta = 27.98^o$. The cluster is located in the constellation Coma Berenices, which is near the Milky Way's north pole. Due to the fact that is located in an area that is not affected by the gas and the dust of the plane of our galaxy, having galactic latitude 87.95 degrees and longtitude 58.08 degrees, makes it easier to be observed and studied. Most of the galaxies that inhabitant the central region of the Coma Cluster are elliptical, while at the outskirts there are several spiral galaxies. In abundance are giant and dwarf ellipticals in the cluster, while the core is dominated by two supergiant elliptical galaxies, the NGC 4874 and the NGC 4889.

Throughout this thesis we assume a flat ($\Omega_m + \Omega_\Lambda = 1$) $\Lambda$CDM model with the cosmological matter density parameter $\Omega_m = 0.3$, consistent with the most recent cosmological results.

In the beginning of our analysis, we downloaded the essential galaxy data in the region of the Abell cluster A1656, from the Sloan Digital Sky Survey Data Release 10. The range covered is a square with right ascension $193 < \alpha < 197$ degrees and declination $26.4 < \delta < 29.6$ degrees. The region contains 839 and for each we downloaded the following parameters: celestial coordinates $(\alpha, \delta)$, redshift, Petrosian magnitudes in the three bands (g,r,i) with their errors, the galaxy ZOO categorization of galactic types (number SP=1 for spiral galaxies and EL=1 for ellipticals), the probability for spiral and elliptical type, the axial ratios b/a in the three bands, based on exponential fits (these parameters are valid only for spirals) and the axis ratio b/a when fitted by De Vaucaluers profile (this is valid only for ellipticals).

In order to identify the galaxy members of the cluster A1656 we set some criteria. We select only the galaxies which fulfill all the following criteria:

- The cluster galaxy members are selected within a specific range of radial velocity. This is a requirement because all the members of the cluster should move at relatively close velocities to each other due to the gravitational interaction among them. In NASA's Ned, the given $1\sigma$ radial velocity of the cluster members of A1656 from the center is 777 $km/s$. In order to select the cluster members, we accept galaxies within $3\sigma$ velocity dispersion from the center, i.e. $\pm 2300$ $km/s$. In this way we can easily exclude background and foreground galaxies. In other words, we select only galaxies within $\pm 0.0077$ from the cluster nominal redshift ($z = 0.0231$).

- The second condition for using galaxies in our analysis, is that their magnitude uncertainties are $\leq 1.5\%$ of the magnitude at all three bands (g,r,i).

- Finally, we select galaxies within different radii fromthe cluster center, depending on the particular study that we are interested in.To this end, we compute for each galaxy the angular separation $\theta$ from the cluster center using the law of cosines and then its spatial distance estimated by:

$$r(i) = D_A \cdot \tan\theta(i) \tag{2.1}$$

  where $D_A = 93.5$ $Mpc$ is the angular diameter distance of the cluster. The maximum distance that we use is 2.5 $h_{72}^{-1}$ $Mpc$, while we consider as the nominal cluster that which corresponds with a radius 1.5 $h_{72}^{-1}$ $Mpc$. Within this radius there are 477 cluster members.

The above procedure, aiming to select and use for our analysis only the galaxies that are specifically cluster members, is obviously very important, in order to come up with accurate and noise-free results.

In order to study the shape of the LF of the different type of galaxies separately, we categorized the galaxies of the cluster into ellipticals, spirals and irregulars using the following criteria:

- As elliptical galaxies we have been selected those with ZOO number El=1. Otherwise if El=0, then elliptical galaxies are those for which the probability of being ellipticals is $\geq$0.6 and the probability of being spirals is $<$0.6.
- As spiral galaxies we identified those for which the ZOO number is SP=1. Otherwise, if SP=0, then spiral galaxies are considered those with probability of being spirals is $\geq$0.6 and having also the probability of being ellipticals is $<$0.6.
- As irregular galaxies we identified those for which the ZOO number is SP=0, EL=0, the probability of being spirals is $<$0.6 and the probability of being ellipticals is $<$0.6.
- The galaxies with both the ZOO numbers EL and SP equal to -1, have not been categorized. Within the radius $1.5h_{72}^{-1}$ $Mpc$, only one galaxy has not been categorized (0.2%) while within the radius $2.5h_{72}^{-1}$ $Mpc$,there are three galaxies that have not been categorized.

## 2.2 Visualisation of the Cluster

Out of the 477 cluster members, within $R = 1.5h_{72}^{-1}\ Mpc$, the elliptical galaxies are 304 constituting the 63.73 % of the galaxies, the spirals are 70 (14.67 %) and the irregulars are 102 (21.38 %).

In order to have a visual idea of the spatial distribution of galaxies within this cluster we plot the distribution of the different types of galaxy members in an equal area projection (Figure 5). The x axis of the plot represents the right ascension multiplied by the cosine of the declination of the cluster center and the y axis represents the declination. In order to visualize better the distribution of the different types of galaxies we plot the ellipticals in red colour, the spirals in blue and the irregulars in green. The galaxy that is not categorized, is plotted as a black square.

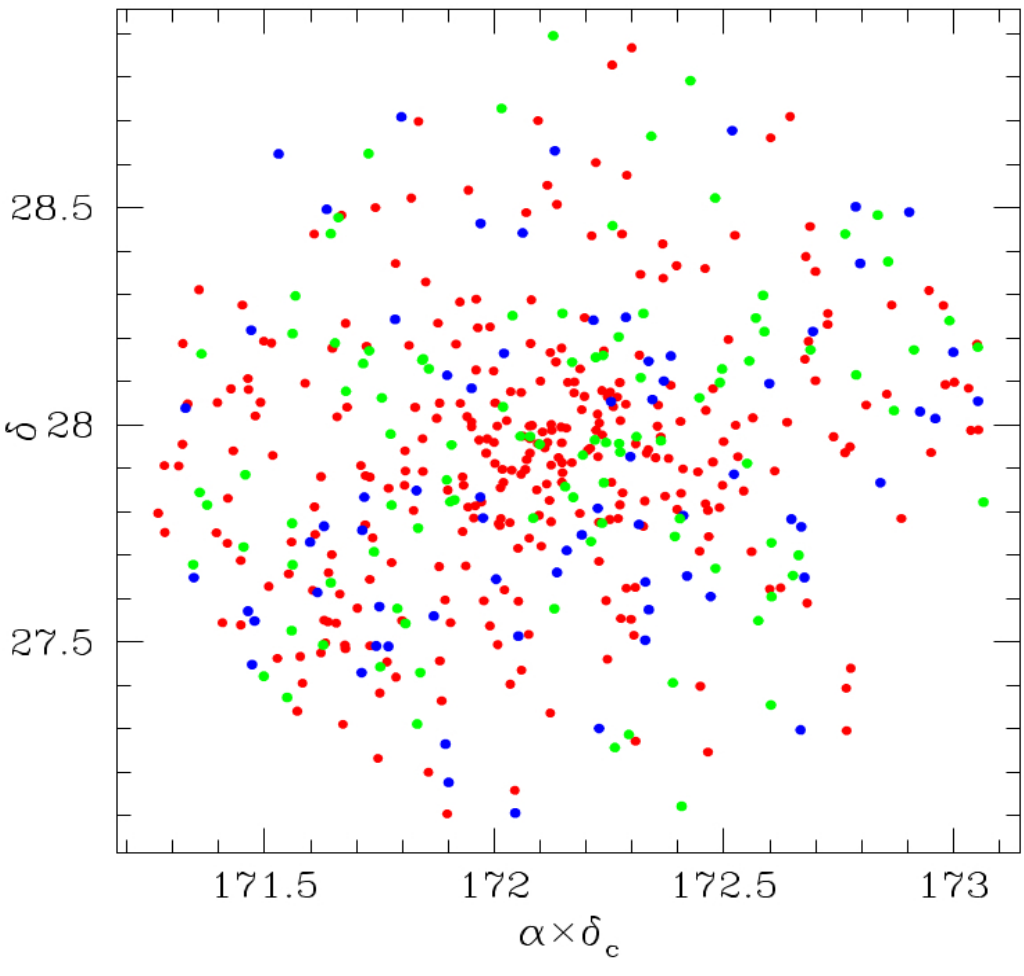


**Figure 5:** . Equal area projection of cluster A1656.

## 2.3 Correcting magnitudes for systematic effects

As we already established, the luminosity function, $\Phi(L)$, of a cluster is the number density of galaxies per luminosity interval. In order to estimate the LF of the Coma cluster, we transform the apparent magnitudes, in the three bands g,r,i of the SDSS galaxies data, into absolute magnitudes using the well-known distance modulus, according to:

$$m_i - M_i = 5\log_{10}[D_L] + 25 + K_i(z) + A_i/sin(b) + A_{int} \tag{2.2}$$

where:

- $m_i$, is the Petrosian apparent magnitude for the three bands (g,r,i). We use Petrosian magnitudes because the galaxies do not have the same radial surface brightness profile. So in order to avoid biases, the SDSS using a form of the Petrosian (1976) system, carries out a measurement for a constant fraction of the total light. This system is independent of galaxy distance.
- $M_i$, is the absolute magnitude (i=g,r,i)
- $D_L$, is the luminosity distance, which for Coma cluster is $D_L = 97.9\ Mpc$.
- $K_i(z)$, is the K-correction for the tree filters (i=g,r,i), which is a function of redshift. This correction is necessary due to the fact that, when we measure the magnitude of the galaxies, at large distance at a specific wavelength $\lambda_o$, the light that we receive is actually emitted from a different part of the spectrum at different redshifts. For that reason the galaxy could be brighter or fainter in this part compared to the benchmark $\lambda_o$ .

  For this procedure, we use the Poggianti's (1997) tabulation of K-correction where it is listed by redshift in bins of variable width. Using a linear interpolation between given redshift values we estimate the K-correction for $z = 0.0231$, in the three bands g,r and i, and for elliptical and spiral galaxies separately (for irregular galaxies we use the same values of k-correction as for spirals).

**Table 1:** K-correction, at $z = 0.0231$, in g, r, i bands for elliptical and spiral galaxies.

| Type | $K_g$ | $K_r$ | $K_i$ |
|---|---|---|---|
| Elliptical | 0.046 | 0.0205 | 0.018 |
| Spiral | 0.03 | 0.0115 | 0.0075 |

- The term $A_i/sin(b)$, is used for correcting the Galactic extinction. The interstellar gas and dust of our Galaxy absorb and scatters light of extragalactic sources. Dust is able to scatter more efficiently the blue light. In this way the background light appears redder. Due to this fact, the distance of the galaxies can be overestimated, increasing the apparent magnitude of the latters, especially at low galactic latitudes. The term $A_i$ is the galactic absorption in the three bands that corrects the magnitude for this effect. We use for this process the values for the $A_i$ given by NASA ned.

**Table 2:** Galactic absorption, $A_i$, in g, r, i bands.

| $A_g$ | $A_r$ | $A_i$ |
|---|---|---|
| 0.027 | 0.019 | 0.014 |

Finally, b, is the galactic latitude which for the Coma cluster is $b = 87.96^o$.

- $A_{int}$, is the internal absorption term, which is necessary only for spiral galaxies. Spiral galaxies due to the dust and gas that they contain, they exhibit absorption and scattering of electromagnetic radiation which depends on the inclination of the disk with respect to the observer. Galaxies with high inclination are affected by more extinction due to the longer path length that light needs to travel. To estimate $A_{int}$ we use the recipe of Pastrav et al. (2013).

## 2.4 Luminosity Function analysis

Having convert the apparent magnitudes, in the three bands, into absolute magnitudes as we analysed in the previous paragraph, we derive the frequency distribution magnitudes in the three bands g,r and i, for the whole cluster, for different radial shells and for different types of galaxies separately.

Subsequently, we use the $\chi^2$ minimization method in order to fit a Schechter luminosity function to each M distribution. Since this is a parametric method we need to decide of the optimal number of magnitude bins. To this end, we vary the number of bins until we obtain the best $\chi^2$. We investigate the range between 6 to 30 bins. Bins more than 30, are dominated by short noise.

Having found the proper number of bins, we perform the $\chi^2$ minimization, living free the three parameters $\alpha$, $M^*$, $\phi^*$ of the Schechter LF:

$$\Phi(M)dM = 0.4 \ln 10 \ \phi^* [10^{-0.4(M-M^*)}]^{\alpha+1} \exp[-10^{-0.4(M-M^*)}] dM$$

Finally we multiply the LF with the volume of the region in which the galaxies existed in order to estimate the $\phi^*$ in correct units.

To this end we estimate the volume of a spherical or shell region of the cluster by measuring the Virial radius, given by (eg., Tovmassian & Plionis 2009):

$$R = \frac{n(n-1)}{\sum_{i=1}^{n-1} \sum_{j=i+1}^{n} [D_L \tan(\delta\theta_{ij})]^{-1}} \tag{2.3}$$

where $D_L$ the luminosity distance and $\delta\theta_{ij}$ the angular (i-j)-pair separation. Then the volume is given by $V = 4\pi R^3/3$.

# 3 Results

In this chapter, we study at first the LF of the whole cluster A1656 within a radius of $1.5h_{72}^{-1}$ Mpc in the tree bands g, r and i. We also estimate the LF for elliptical, spiral and irregular galaxies separately in order to evince and evaluate the differences in the functional form. In order to make a deeper study of the estimated LF's parameters $\alpha$, $M^*$ and investigate possible dependencies among the parameters, we plot within the $3\sigma$ and $1\sigma$ contorts. We also study separately the core region of the cluster within a radius $R = 1h_{72}^{-1}$ Mpc, the shell region with $1h_{72}^{-1}$ Mpc $\leq R \leq 2.5h_{72}^{-1}$ Mpc and the outskirts of the cluster at a region $1.75h_{72}^{-1}$ Mpc $\leq R \leq 2.5h_{72}^{-1}$ Mpc. We perform this independently for all different kind of galaxies aiming to investigate a possible difference in their LF also as a function of a different region of the cluster. Finally, we study the dependence of the LF's parameters $\alpha$, $M^*$ on radial distance from the cluster center.

## 3.1 Luminosity Function of the Cluster at $R = 1.5h_{72}^{-1}$ Mpc

In order to have a picture of galaxy magnitude distribution we present the combined histograms (using 20 bins with width 0.5), in each of the three bands, as well as for each type of galaxies.

As we mentioned above, the cluster members are within this radius 477. The elliptical galaxies are 304 ( 63.73 % of the galaxies), the spiral galaxies are 70 (14.67 %) and the irregulars are 102 ( 21.38 %). The virial radius of this region is $R = 1.39$ Mpc and the volume is $V = 11.3$ Mpc$^3$. The number density of the galaxies in this volume is $n = 42.21$ Galaxies Mpc$^3$, the number density for elliptical galaxies is $n = 26.9$ Galaxies Mpc$^3$, for spirals $n = 6.19$ Galaxies Mpc$^3$ and for irregulars $n = 9.02$ Galaxies Mpc$^3$.

In order to derive the parameters of the luminosity function $\alpha$, $M^*$, $\phi^*$, for the whole sample and for all types of galaxies in the three bands we follow for each band the following procedure: first, we choose the number of magnitude bins to be such as to give the best $\chi^2$ (as we have already estimated). We eliminate the bins that have central value approximately greater than -17.77, because galaxies with corresponding value or

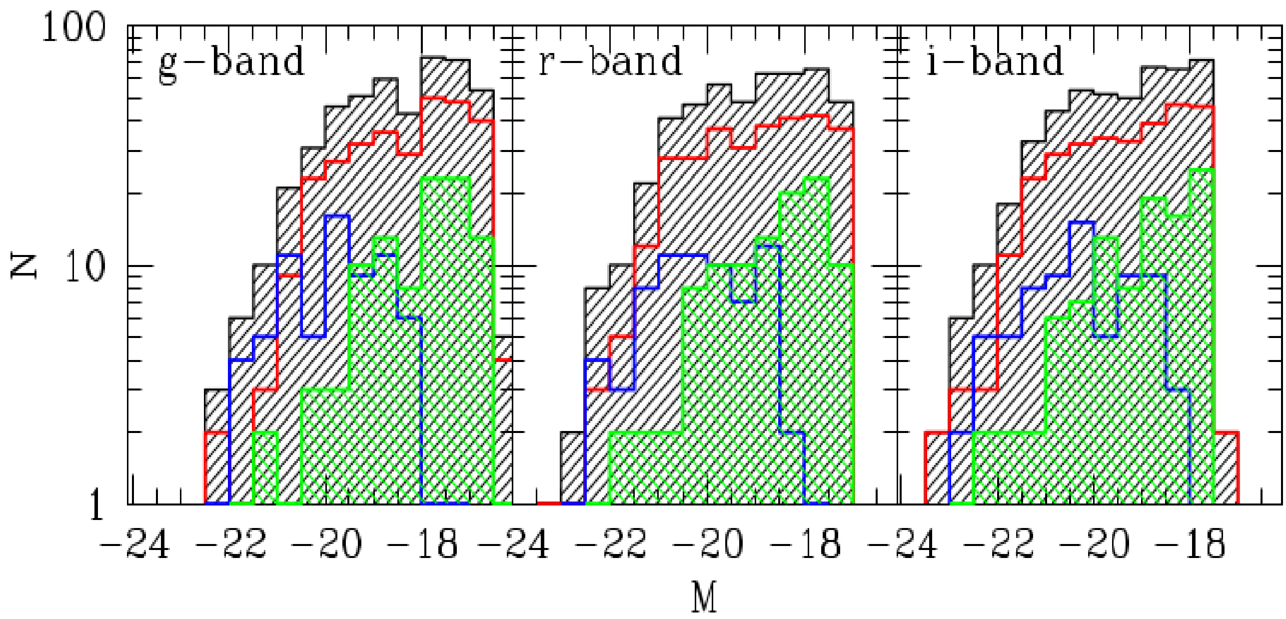


**Figure 6:** Combined histograms, in g, r, i bands, of the absolute magnitude distribution of the Coma cluster's galaxies. The black histogram corresponds to the whole sample, the red, blue and green to elliptical, spiral and irregular galaxies, respectively. We can see a lack of very faint spirals, as expected since no dwarf spirals have been ever observed.

fainter are not within the completeness limit of the SDSS spectroscopic sample. Next, we search for the best fitted LF through the $\chi^2$ minimization procedure leaving free the three parameters. The range of values that we use are the following: for $\alpha \in [-4, -0.5]$ with a step size of 0.01, for $M^* \in [-30, -17]$ with a step size of 0.01 and for $\phi^* \in [0, 9]$ with a step size of 0.1. $N_f$ is the different free parameters ($N_f$= 2 or 3 for our analysis) and the degrees of freedom are $d.o.f = n_b - N_f$, where $n_b$ is the number of selected bins that taken into account for $\chi^2$ estimation. As we can see from Table 10, for $N_f = 3$ we have the $1\sigma$ (68.3%) confidence level for $\Delta\chi \leq$ 3.53. At Figure 7 we present the r-band absolute magnitude histograms and the fitted LFs for the whole sample of galaxies and for the three types separately, while for the other bands g and i the results can be found in the Appendix B. Our results for the best fitting LF parameters, in the three filters, for all galaxies and the different galaxy types presented in Table 3.

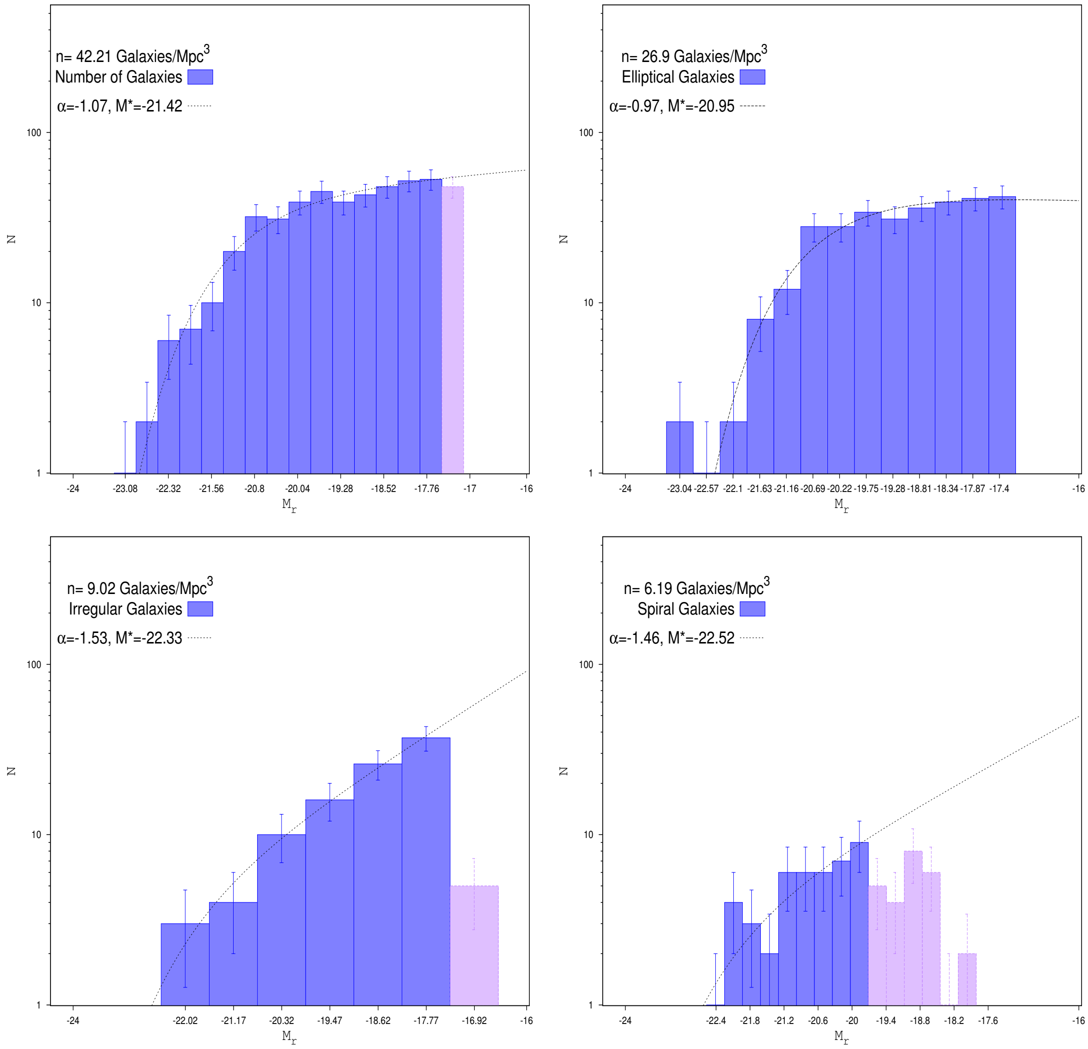


**Figure 7:** Galaxy luminosity functions in the r-band, for a radius $R = 1.5h_{72}^{-1}$ Mpc from the cluster's center. *Left upper panel*: the whole sample of galaxies. *Right upper panel*: elliptical galaxies. *Left bottom panel*: irregular galaxies. *Right bottom panel*: spiral galaxies. The purple bins are those that have been eliminated from the analysis.

**Table 3:** Best fit Schechter parameters in the three bands g, r, i, for the whole sample of galaxies and for the different types of galaxies separately, within a cluster radius of $R = 1.5h_{72}^{-1}$ Mpc. The uncertainty of the parameters $\alpha$ and $M^*$, is the range for which $\Delta\chi^2 \leq 2.3$ when the parameter $\phi^*$ is kept fixed at its best value.

| Band | Type | $\alpha$ | $M^*$ | $\phi^*[h^3\ Mpc^{-3}]$ | $\chi^2/d.o.f$ |
|---|---|---|---|---|---|
| g | All Galaxies | $-1.07^{+0.035}_{-0.031}$ | $-20.79^{+0.158}_{-0.147}$ | 3.70 | 0.44 |
| | Ellipticals | $-0.97^{+0.070}_{-0.059}$ | $-20.19^{+0.155}_{-0.168}$ | 4.50 | 0.47 |
| | Irregulars | $-1.43^{+0.097}_{-0.064}$ | $-20.35^{+0.267}_{-0.236}$ | 0.70 | 0.89 |
| | Spirals | $-0.96^{+0.131}_{-0.095}$ | $-21.69^{+0.517}_{-0.710}$ | 1.10 | 0.34 |
| r | All Galaxies | $-1.07^{+0.034}_{-0.031}$ | $-21.42^{+0.155}_{-0.143}$ | 4.10 | 0.47 |
| | Ellipticals | $-0.97^{+0.044}_{-0.039}$ | $-20.95^{+0.171}_{-0.158}$ | 4.42 | 0.54 |
| | Irregulars | $-1.53^{+0.049}_{-0.042}$ | $-22.33^{+0.287}_{-0.259}$ | 0.40 | 0.22 |
| | Spirals | $-1.46^{+0.154}_{-0.115}$ | $-22.52^{+0.581}_{-0.782}$ | 0.30 | 0.48 |
| i | All Galaxies | $-1.11^{+0.031}_{-0.029}$ | $-21.86^{+0.154}_{-0.143}$ | 3.90 | 0.44 |
| | Ellipticals | $-1.04^{+0.036}_{-0.040}$ | $-21.54^{+0.176}_{-0.164}$ | 3.00 | 0.70 |
| | Irregulars | $-1.51^{+0.046}_{-0.047}$ | $-22.52^{+0.271}_{-0.279}$ | 0.30 | 0.10 |
| | Spirals | $-1.25^{+0.164}_{-0.129}$ | $-22.52^{+0.430}_{-0.416}$ | 0.60 | 0.69 |

As we can see, for the whole sample of galaxies and for ellipticals, which dominate the cluster, a standard Schechter function provides a satisfactory fit to the data dropping steeply at bright magnitudes and rises gradually at fainter magnitudes (Schechter 1976), while for irregular and spiral galaxies the fit is not that good due to the fact that the number of galaxies is small. Nonetheless, we can notice that for irregular and spiral galaxies, the LF has a steeper faint-end slope in the r and i band. It is also noteworthy that the characteristic $M^*$ brightens systematically going from the g to r and then the i band as expected from the fact that red galaxies dominate the cluster potential. Lopez-Cruz et al. (1997) propose that the flat faint-end slope of the LFs in rich clusters like, Coma cluster, is a result of the disruption of dwarf galaxies. Beijersbergen et al. (2002), performing a similar study, estimated the corresponding Coma cluster LF parameters to be $\alpha = -1.16^{+0.012}_{-0.019}$ and $M^* = -21.58^{+0.12}_{-0.17}$ (after converting for $h = 0.72$), consistent with our results. Also, Loveday et al. (2012) estimated, assuming a Hubble constant of $H_0 = 100h\ km/s/Mpc$ and $\Omega_m = 0.3$, the LF's parameters for 12860 low-redshift field galaxies at the r-band: $\alpha = -1.26 \pm 0.02$ and $M^* - 5\log h = -20.73 \pm 0.03$. This latter study can be used to compare results of our Coma cluster LF to that of field galaxies.

Finally, keeping fixed the value of $\phi^*$ (we use the value that revealed through the $\chi^2$ minimization procedure for three free parameters) and having now only two free parameters using the range of values: for $\alpha \in [-5, -0.5]$ with a step size of 0.001 and for $M^* \in [-40, -15]$ with a step size of 0.001. We provide the $1\sigma$ and $3\sigma$ uncertainties contour plots of the two fitted parameters at Figure 8 where are showed the results for all galaxies in the sphere with $R = 1.5h_{72}^{-1}$ Mpc and for the different types of galaxies as well. For $N_f = 2$ the $1\sigma$ (68.3%) confidence level corresponds to $\Delta\chi^2 \leq 2.3$ while the $3\sigma$ error corresponds to $\Delta\chi^2 \leq 11.83$. It is notable that for the whole sample of galaxies, the range of $1\sigma$ and $3\sigma$ is very narrow, indicating a good fit of the Schechter model, while for the irregular and especially for the spiral galaxies the degeneracies among the parameters are large since all the combinations of $\alpha$ and $M^*$ within the $1\sigma$ contour are equally possible.

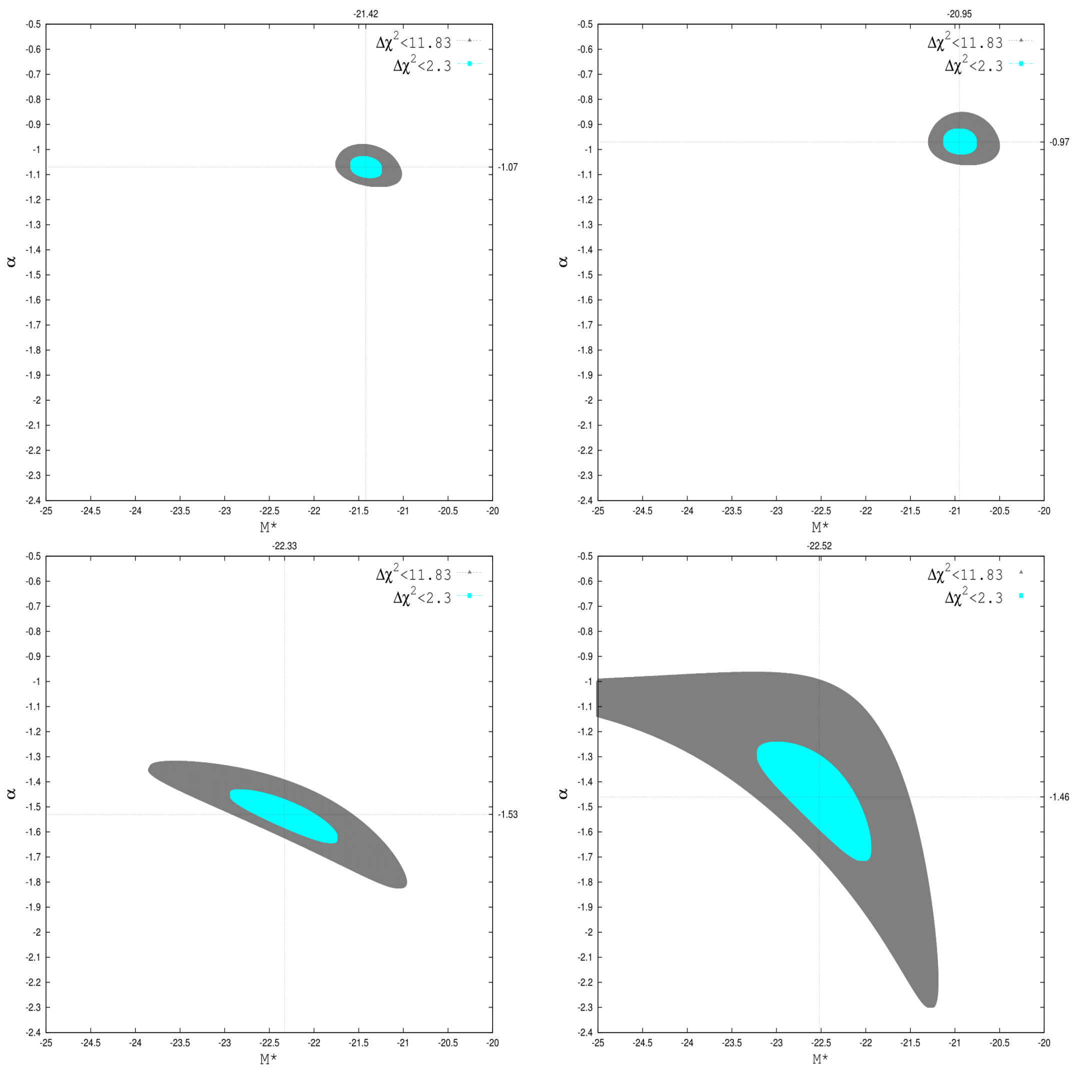


**Figure 8:** Solution space for $\alpha$ and $M^*$, in the r-band, within a radius $R = 1.5h_{72}^{-1}$ Mpc. The blue contour corresponds to the $1\sigma$ confidence level (68.3%) and the grey to the $3\sigma$ confidence level (99.73%). The best-fit values are at the intersections of the dashed lines. *Left upper panel*: the whole sample of galaxies. *Right upper panel*: elliptical galaxies. *Left bottom panel*: irregular galaxies. *Right bottom panel*: spiral galaxies.

## 3.2 Luminosity Function of the core and the outskirts of the cluster

In this paragraph we intent to study the form of the LF in the core region of the cluster, where the galaxies are expected to have a different formation history than the galaxies in the outskirts of the cluster. This should be reflected in differently shaped LFs for these regions due to the fact that they are dominated by different types of galaxies while the density of the various regions is significantly different.

We wish to study the core region at $R = 1h_{72}^{-1}$ Mpc, the shell region $1h_{72}^{-1}$ Mpc $\leq R \leq 2.5h_{72}^{-1}$ Mpc and the outskirts of the cluster $1.75h_{72}^{-1}$ Mpc $\leq R \leq 2.5h_{72}^{-1}$ Mpc. In Table 4 are given the volume, the number of galaxies and the number of different types of galaxies with the percentage of each type for the different regions studied.

**Table 4:** The volume and the number of galaxies with their percentages (for each type), in the three regions of the cluster.

| Region [Mpc] | Vol.[Mpc$^3$] | $N_{gals}$ | Ellipticals (%) | Irregulars(%) | Spirals(%) |
|---|---|---|---|---|---|
| $R = 1$ | 3.88 | 318 | 214 (67.3%) | 62 (19.5%) | 41 (12.89%) |
| $1 \leq R \leq 2.5$ | 30.02 | 317 | 196 (52.83%) | 96 (25.88%) | 77 (20.75%) |
| $1.75 \leq R \leq 2.5$ | 19.99 | 151 | 75 (49.67%) | 39 (25.83%) | 35 (23.18%) |

In order to derive the parameters of the luminosity function $\alpha$, $M^*$, $\phi^*$, for the whole sample of galaxies and for the different galaxy types, in the g,r and i bands and for the three selected regions, we follow the exact same procedure used previously. The results for each region are presented in the Table 5, Table 6 and Table 7 respectively. The histograms and the fitted LFs, in the r-band, for the whole sample of galaxies and for the three types of galaxies separately are showed in Figure 9 , 10 and 11 (the corresponding figures for the g and i bands can be found in Appendix C).

**Table 5:** Best fit Schechter parameters in the three bands g, r, i, for the whole sample of galaxies and for the different type of galaxies separately, within a cluster radius $R = 1h_{72}^{-1}$ Mpc. The uncertainty of the parameters $\alpha$ and $M^*$ is the range for which $\Delta\chi^2 \leq 2.3$, when keeping the parameter $\phi^*$ fixed at its best value.

| Band | Type | $\alpha$ | $M^*$ | $\phi^*[h^3\ Mpc^{-3}]$ | $\chi^2/d.o.f$ |
|---|---|---|---|---|---|
| g | All Galaxies | $-1.07^{+0.047}_{-0.043}$ | $-20.64^{+0.179}_{-0.160}$ | 8.90 | 0.54 |
| | Ellipticals | $-1.01^{+0.082}_{-0.070}$ | $-20.31^{+0.224}_{-0.200}$ | 8.90 | 0.49 |
| | Irregulars | $-1.01^{+0.163}_{-0.127}$ | $-19.37^{+0.344}_{-0.276}$ | 6.50 | 0.54 |
| | Spirals | $-1.62^{+0.187}_{-0.131}$ | $-21.86^{+0.460}_{-0.365}$ | 0.60 | 0.25 |
| r | All Galaxies | $-1.04^{+0.038}_{-0.034}$ | $-21.31^{+0.185}_{-0.167}$ | 8.70 | 0.26 |
| | Ellipticals | $-1.01^{+0.053}_{-0.046}$ | $-20.95^{+0.208}_{-0.181}$ | 6.80 | 0.39 |
| | Irregulars | $-0.95^{+0.174}_{-0.135}$ | $-19.86^{+0.342}_{-0.275}$ | 5.30 | 0.53 |
| | Spirals | $-1.28^{+0.259}_{-0.176}$ | $-21.68^{+0.488}_{-0.413}$ | 1.80 | 0.48 |
| i | All Galaxies | $-1.08^{+0.042}_{-0.038}$ | $-21.70^{+0.184}_{-0.165}$ | 8.40 | 0.47 |
| | Ellipticals | $-1.10^{+0.045}_{-0.040}$ | $-21.63^{+0.215}_{-0.190}$ | 8.90 | 0.62 |
| | Irregulars | $-0.85^{+0.164}_{-0.128}$ | $-20.06^{+0.340}_{-0.267}$ | 6.30 | 0.49 |
| | Spirals | $-1.71^{+0.126}_{-0.091}$ | $-23.54^{+0.456}_{-0.347}$ | 0.30 | 0.68 |

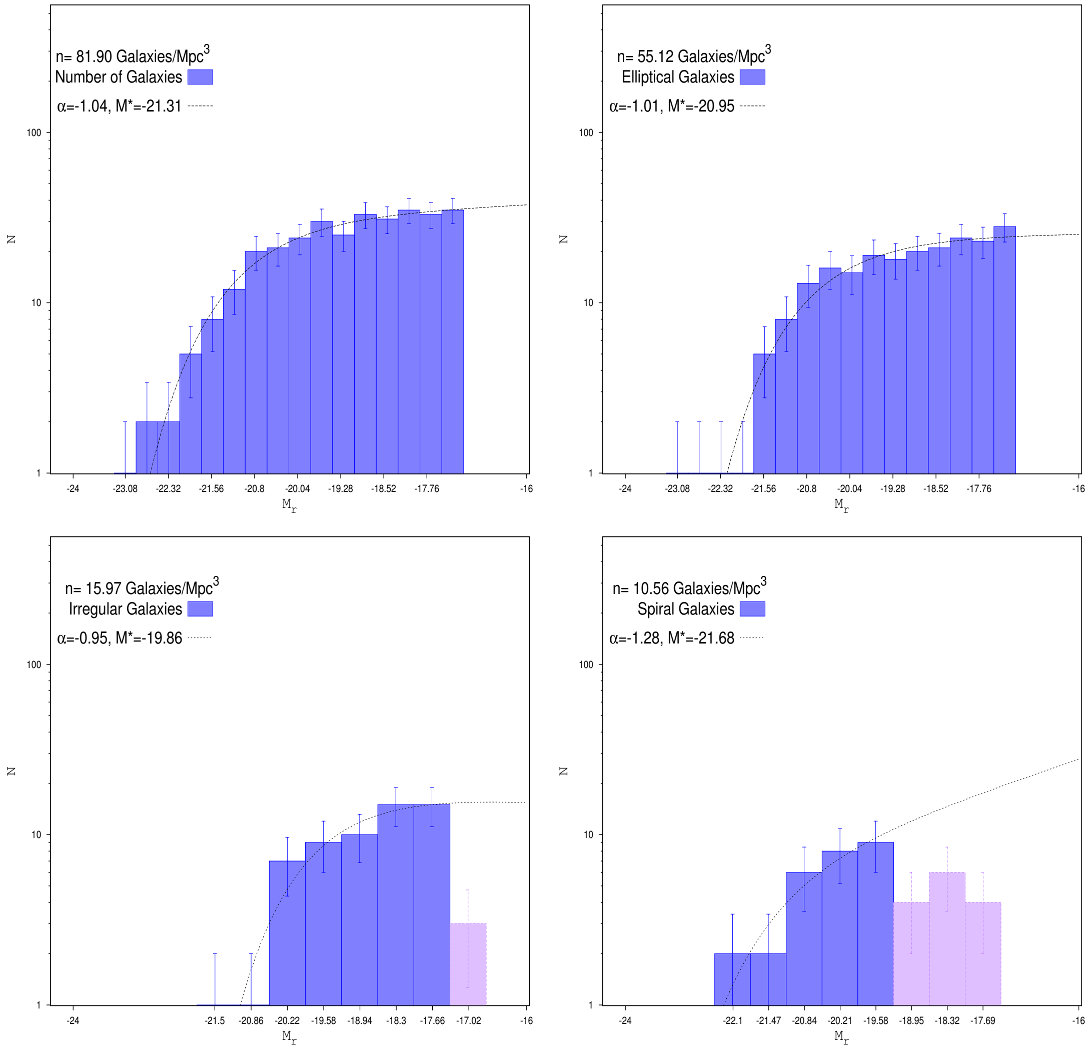


**Figure 9:** Galaxy luminosity functions of the core region of the cluster, in the r-band, within a radius $R = 1h_{72}^{-1}$ Mpc. *Left upper panel*: the whole sample of galaxies. *Right upper panel*: elliptical galaxies. *Left bottom panel*: irregular galaxies. *Right bottom panel*: spiral galaxies. The purple bins are those that have been eliminated from the analysis.

**Table 6:** Best fit Schechter parameters in the three bands g, r, i, for the whole sample of galaxies and for the different type of galaxies separately, within the shell region $1h_{72}^{-1}$ Mpc $\leq R \leq 2.5h_{72}^{-1}$ Mpc. The uncertainty of the parameters $\alpha$ and $M^*$ is the range for which $\Delta\chi^2 \leq 2.3$ when keeping the parameter $\phi^*$ fixed at its best value.

| Band | Type | $\alpha$ | $M^*$ | $\phi^*[h^3\ Mpc^{-3}]$ | $\chi^2/d.o.f$ |
|---|---|---|---|---|---|
| g | All Galaxies | $-1.08^{+0.040}_{-0.036}$ | $-20.87^{+0.188}_{-0.176}$ | 0.90 | 1.10 |
| | Ellipticals | $-0.93^{+0.089}_{-0.077}$ | $-20.12^{+0.231}_{-0.214}$ | 1.20 | 0.78 |
| | Irregulars | $-1.53^{+0.070}_{-0.058}$ | $-20.97^{+0.288}_{-0.251}$ | 0.10 | 0.62 |
| | Spirals | $-1.29^{+0.049}_{-0.040}$ | $-23.06^{+0.664}_{-0.581}$ | 0.10 | 0.58 |
| r | All Galaxies | $-1.09^{+0.033}_{-0.029}$ | $-21.55^{+0.184}_{-0.170}$ | 1.00 | 0.59 |
| | Ellipticals | $-1.00^{+0.056}_{-0.049}$ | $-21.04^{+0.243}_{-0.226}$ | 0.60 | 0.62 |
| | Irregulars | $-1.43^{+0.071}_{-0.059}$ | $-21.25^{+0.319}_{-0.280}$ | 0.10 | 0.67 |
| | Spirals | $-1.07^{+0.072}_{-0.058}$ | $-21.86^{+0.656}_{-0.813}$ | 0.30 | 0.64 |
| i | All Galaxies | $-1.10^{+0.034}_{-0.030}$ | $-22.01^{+0.207}_{-0.200}$ | 0.80 | 0.80 |
| | Ellipticals | $-1.02^{+0.053}_{-0.046}$ | $-21.51^{+0.247}_{-0.227}$ | 0.70 | 0.50 |
| | Irregulars | $-1.44^{+0.052}_{-0.043}$ | $-22.43^{+0.338}_{-0.300}$ | 0.10 | 0.55 |
| | Spirals | $-1.07^{+0.071}_{-0.057}$ | $-22.20^{+0.657}_{-0.812}$ | 0.30 | 0.73 |

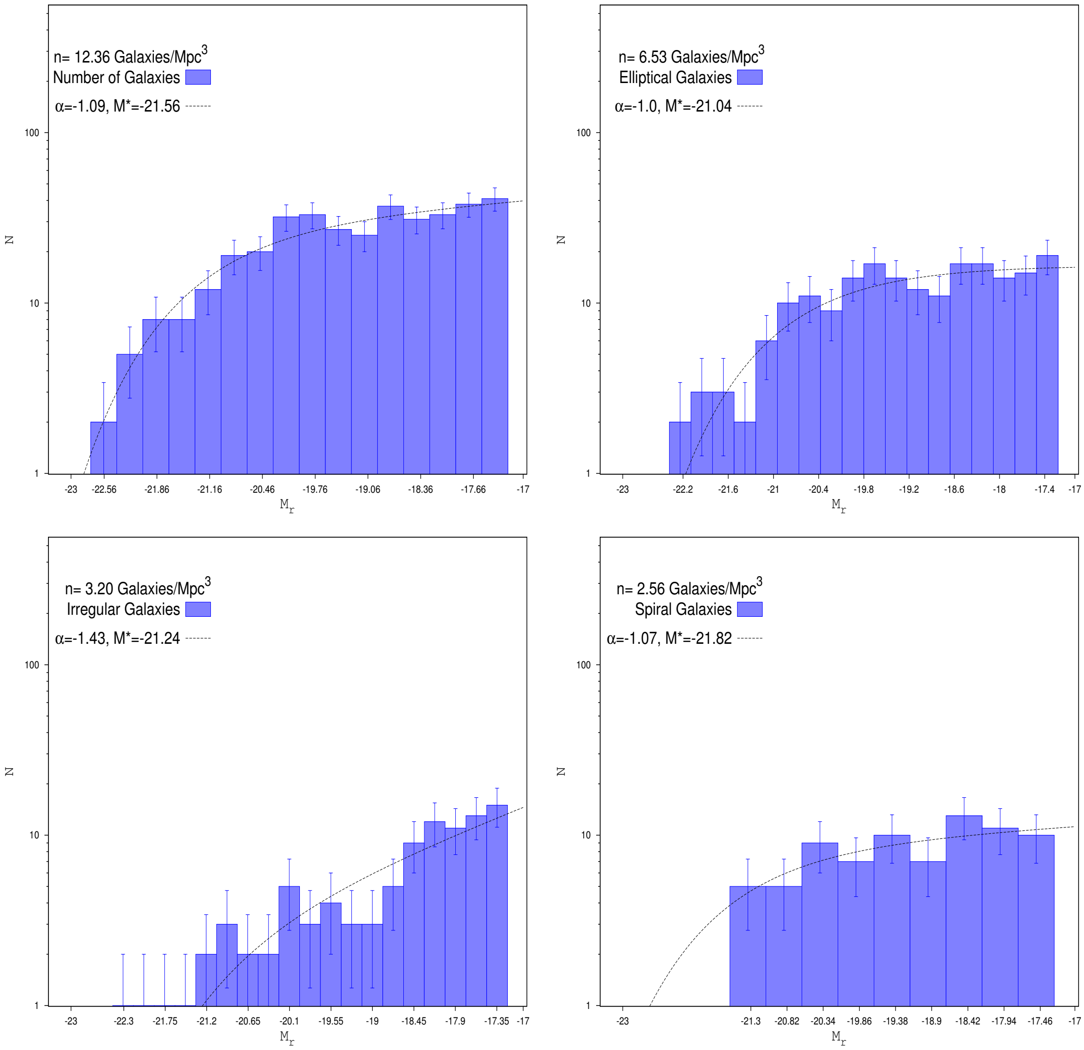


**Figure 10:** Galaxy luminosity functions, in the r-band, of the shell region: $1h_{72}^{-1}$ Mpc $\leq R \leq 2.5h_{72}^{-1}$ Mpc. *Left upper panel*: the whole sample of galaxies. *Right upper panel*: elliptical galaxies. *Left bottom panel*: irregular galaxies. *Right bottom panel*: spiral galaxies.

**Table 7:** Best fit Schechter parameters (for the three bands g, r, i) for the whole sample and for the different types of galaxies separately, within a cluster's shell region $1.75h_{72}^{-1}$ Mpc $\leq R \leq 2.5h_{72}^{-1}$ Mpc. The uncertainty of the parameters $\alpha$ and $M^*$ is the range for which $\Delta\chi^2 \leq 2.3$ when keeping the parameter $\phi^*$ fixed at its best value.

| Band | Type | $\alpha$ | $M^*$ | $\phi^*[h^3\ Mpc^{-3}]$ | $\chi^2/d.o.f$ |
|---|---|---|---|---|---|
| | All Galaxies | $-1.10^{+0.050}_{-0.042}$ | $-21.18^{+0.330}_{-0.313}$ | 0.80 | 0.60 |
| g | Ellipticals | $-1.00^{+0.095}_{-0.074}$ | $-20.43^{+0.440}_{-0.411}$ | 0.70 | 0.58 |
| | Irregulars | $-1.57^{+0.119}_{-0.086}$ | $-21.17^{+0.481}_{-0.382}$ | 0.10 | 0.28 |
| | Spirals | $-1.35^{+0.161}_{-0.111}$ | $-21.28^{+0.740}_{-0.620}$ | 0.10 | 0.77 |
| | All Galaxies | $-1.20^{+0.049}_{-0.043}$ | $-21.76^{+0.304}_{-0.279}$ | 0.50 | 0.81 |
| r | Ellipticals | $-1.17^{+0.072}_{-0.058}$ | $-21.82^{+0.506}_{-0.479}$ | 0.40 | 0.63 |
| | Irregulars | $-1.51^{+0.087}_{-0.065}$ | $-21.90^{+0.479}_{-0.392}$ | 0.10 | 0.27 |
| | Spirals | $-1.26^{+0.101}_{-0.073}$ | $-22.26^{+0.870}_{-0.800}$ | 0.10 | 0.61 |
| | All Galaxies | $-1.19^{+0.048}_{-0.041}$ | $-22.07^{+0.339}_{-0.326}$ | 0.50 | 0.90 |
| i | Ellipticals | $-1.01^{+0.091}_{-0.071}$ | $-21.59^{+0.457}_{-0.438}$ | 0.60 | 0.71 |
| | Irregulars | $-1.50^{+0.088}_{-0.066}$ | $-22.16^{+0.497}_{-0.406}$ | 0.10 | 0.49 |
| | Spirals | $-1.27^{+0.099}_{-0.071}$ | $-22.84^{+0.951}_{-0.844}$ | 0.10 | 1.43 |

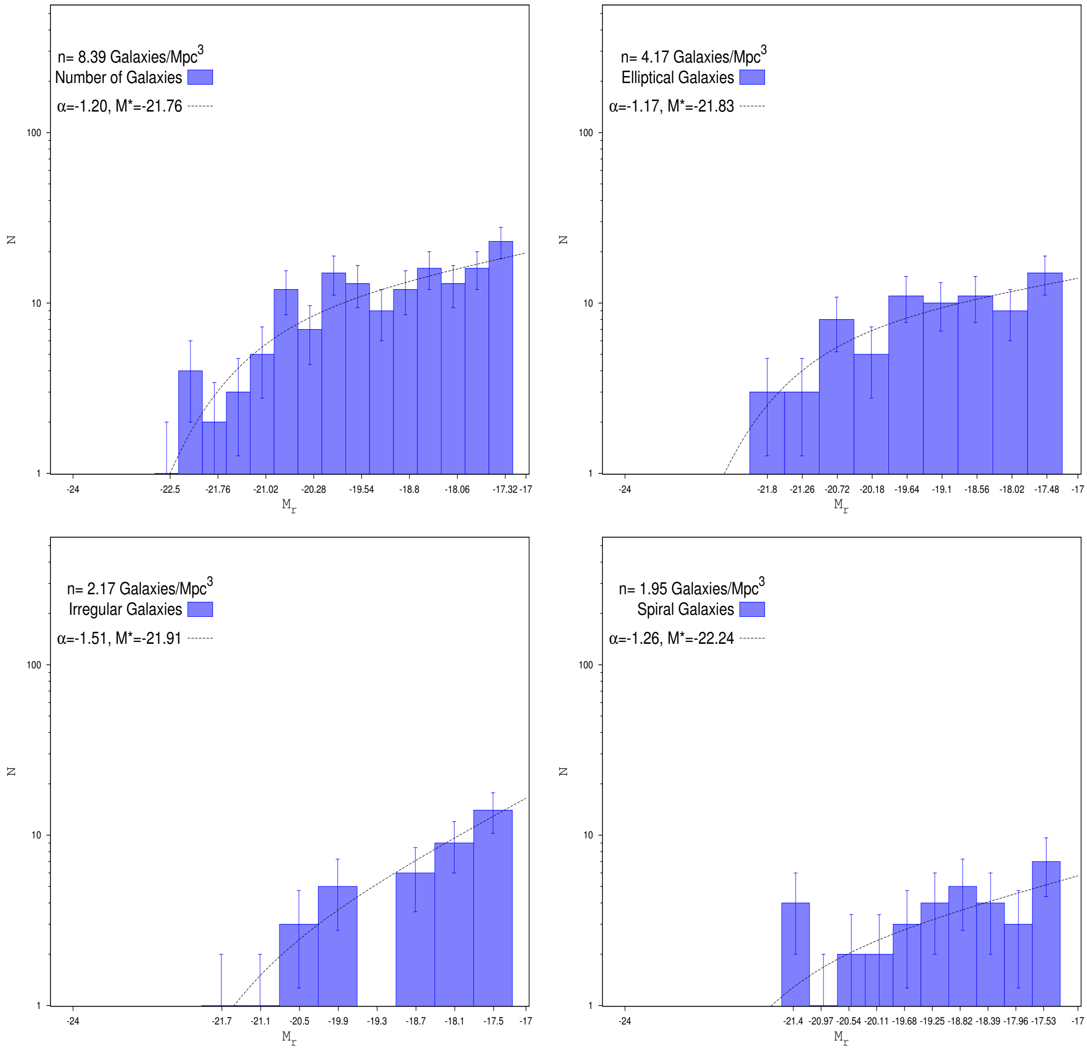


**Figure 11:** Galaxy luminosity functions, in the r-band, for the cluster shell $1.75h_{72}^{-1}$ Mpc $\leq R \leq 2.5h_{72}^{-1}$ Mpc. *Left upper panel*: the whole sample of galaxies. *Right upper panel*: elliptical galaxies. *Left bottom panel*: irregular galaxies. *Right bottom panel*: spiral galaxies.

We can see from the tables and the figures above that there is an increase, in r and g band, in the faint-end slope of the LF from the core toward the outskirts. This happens due to the fact that at the outskirts the fraction of faint galaxies increases. We can also notice that in the core, the irregular's and spiral's do not provide good fit to the Schechter function due to the small number of galaxies. At the outskirts we can obtain better fits of the LF due to their relatively higher galaxy density of spirals and irregulars. Additionally the parameter $M^*$ is brighter in the outskirts than in the core.

## 3.3 The dependence of the LF's parameters $\alpha$, $M^*$ on cluster-centric distance

In this chapter we intent to study the dependence of the two parameters $\alpha$ and $M^*$ on the radial distance from the cluster center. To this end, we separate our galaxy sample in the four radial regions that are presented in Table 8, where the volume, the total number of galaxies and the number of the different galaxy types are showed.

After separating our sample in the radial regions we perform the same procedure that we use in the previous paragraphs, in order to estimate the parameters $\alpha$ and $M^*$. The results for the four regions are presented in Table 10, 11, 12 (that can be found in Appendix D) and Table 7, respectively.

**Table 8:** The volume and the number of galaxies with their percentages (for each type), in the four regions of the cluster.

| Region [Mpc] | Vol.[Mpc$^3$] | $N_{gals}$ | Ellipticals (%) | Irregulars(%) | Spirals(%) |
|---|---|---|---|---|---|
| $R = 0.5$ | 0.77 | 166 | 120 (72%) | 27 (16.26%) | 17 (10.24%) |
| $0.5 < R \leq 1$ | 3.11 | 152 | 94 (61.84%) | 33 (21.71%) | 24 (15.79%) |
| $1 < R \leq 1.75$ | 12.03 | 220 | 121 (55%) | 57 (25.9%) | 42 (19.09%) |
| $1.75 < R \leq 2.5$ | 19.99 | 151 | 75 (49.67%) | 39 (25.83%) | 35 (23.18%) |

In order to have an idea of the dependence of the LF parameters with cluster-centric distance, we produce, for the r-band, the dependence of the parameter $\alpha$ and $M^*$ on the radius $R$ (Figure 12). The error bars are included only for the irregulars to avoid overcrowding. The values of the uncertainties for the two parameters $\alpha$ and $M^*$ can be found in in Table 10, 11, 12 and 7.

As we can see at Figure 12 the slope $\alpha$ of the LF is the flattest for the whole sample of galaxies, for ellipticals and spirals at the shell region $1 < R \leq 1.75h_{72}^{-1}$ Mpc. The faint end slope is steeper at the outskirts of the cluster for all galaxy types ( note that for spirals the fit at $0.5 < R \leq 1h_{72}^{-1}$ Mpc is very bad and the results are not showed).

The characteristic magnitude $M^*$, for the r-band, is brighter in the core region (within

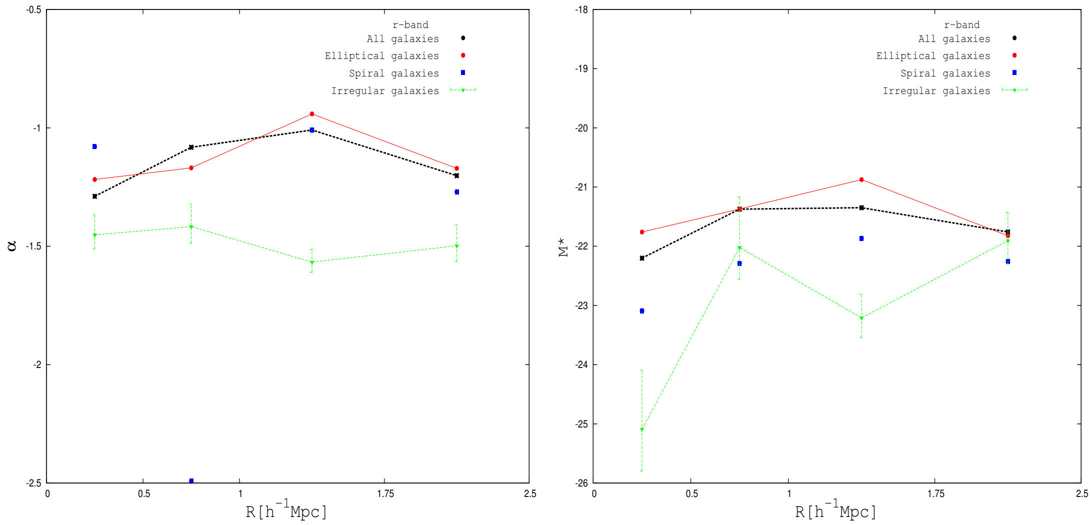


**Figure 12:** The dependence of the LF's parameters $\alpha$, $M^*$ on cluster-centric distance, in the r-band. *Left panel*: The dependence of the $\alpha$ parameter on cluster-centric distance. *Right panel*: The dependence of $M^*$ parameter on cluster-centric distance.

a radius of $R = 0.5h_{72}^{-1}$ Mpc ) for all of our samples, due to the fact that the core region is dominated by giant elliptical galaxies. Fainter $M^*$ values are found in the $1 < R \leq 1.75h_{72}^{-1}$ Mpc region, while the uncertainties of both $\alpha$ and $M^*$, for spirals and irregulars, are quite large. However,the brightest $M^*$ values appear to be of the irregulars and the spirals in the core region but these are unreliable results due to extremely small number of corresponding galaxies in this region. The same results apply for the g and i band.

The steepening of the faint-end of the LF towards the outskirts, where the number density is small, indicates the existence of environmental effects. The difference of the shape of the LF as a function of cluster-centric distance indicates changes in the galaxy population mix. This could lead to the conclusion that, while a steeper faint end slope in the outskirts indicates a greater percentage of faint galaxies, in the virialized core region where galaxies have already been processed via mergers and interactions the faint-end LF is flatter.

Inspecting also Table 8, where we see clearly that the spiral and irregular fraction is significantly higher at the cluster outskirts with respect to the cluster core, we conclude that their interactions eventually lead not only to a higher fraction of elliptical galaxies but also to brighter galaxies.

# 4 Conclusions

In this thesis we studied the LF of galaxies in the Coma rich cluster of galaxies. We have first identified the cluster members from the SDSS DR10 spectroscopic galaxy catalogue, applying all the necessary corrections (K-corection, Galactic and internal absorption) to the apparent magnitudes (in g, r and i bands). We then estimated the LF of the cluster within radius $R = 1.5h_{72}^{-1}$ Mpc for the whole sample of galaxies, comparing the results with the field LF, and separately for ellipticals, spirals and irregulars as well. We notice that a single Schechter function provides a relatively good fit to our samples. As expected ellipticals shape the LF of the whole sample of galaxies, due to the fact that they are more numerous, especially in the cluster's core region. Next, in order to study the environmental dependence of the different galaxy types, we estimate the LF's parameters $\alpha$ and $M^*$ in the core and the outskirts of the cluster. We notice that the faint end slope of the LF steepens towards the outskirts. Unfortunately, the fits for irregulars and spirals are not very reliable since their numbers are very small and thus we cannot derive strong conclusions. Finally we study the dependence of the two LF parameters on the radial distance from the cluster center. Also this analysis shows the presence of clear environmental effects that alter the shape of the LF, leading to a steeper faint-end slope at the outskirts and to flat faint-end slope towards the core region. Physical processes, like mergers, interactions and tidal stripping of the IGM gas, that alter the population mix as a function of cluster-centric distance and alter also the galaxy luminosities, are most probably the causes of the observed LF differences.

# 5 References


Andreon, S., Maughan, B., Trinchieri, G., & Kurk, J. 2009, A&A, 507, 147

Aragón-Calvo, M. A. et al. 2010 MNRAS, 404, L89

Aragón-Calvo, M. A., van de Weygaert, R., Jones, B. J. T. 2010 MNRAS, 408, 2163A

Bahcall, N. A., Batuski, D.J., Olowin, R.P. 1988, ApJ, 333, L13

Bahcall, N. A., Lubin, L M., & Dorman, V. 1995, ApJ, 447, L81

Bahcall, N. A., & Oh, P. 1996, ApJ, 462, L43

Bautz L., Morgan W.W., 1970, ApJ, 162, L149

Betoule M. et al., 2014, ArXiv e-prints

Beijersbergen, M., Hoekstra, H., van Dokkum, P. G., & van der Hulst, T. 2002, MNRAS, 329, 385

Bond, J.R., Efstathiou, G., Silk, J. 1980. Phys. Rev. Lett. 45: 1980

Chon, G., B?hringer, H., Collins, C. A., & Krause, M. 2014, A& A, 567, A144

Coil, A. L. 2012, arXiv:1202.6633

Dressler, A. 1980, ApJ, 236, 351

Dressler, A., Oemler, Jr., A., Couch, W. J., et al. 1997, ApJ, 490,577

Ferrari C., Govoni F., Schindler S., Bykov A.M. & Rephaeli Y. (2008), arXiv:0801.0985, doi:10.1007/s11214-008-9311-x

Forman, W., Jones, C., Markevitch, M., Vikhlinin, A., & Churazov, E. 2002, arXiv:astro-ph/0207165

Hansen S. M., McKay T. A., Wechsler R. H., Annis J., Sheldon E. S., Kimball A., 2005, ApJ, 633, 122

Jones B. J. T., van de Weygaert R., Aragon-Calvo M. A., 2010, MNRAS, 408, 897

Laub, C. & Kuhl, T. *A Critical Look at the Fitting of Reflectivity Models using the Reduced Chi-Square Statistic.* Retrieved from http://neutrons.ornl.gov

Loveday, J. et al. 2012, MNRAS, 420, 1239-1262

Montero-Dorta, A. D., & Prada, F. 2009, MNRAS, 399, 1106

Mulchaey J.S. (2000), ARAA, 38, 289

Newman, A. B., Ellis, R. S., Andreon, S., Treu, T., Raichoor, A., and Trinchieri, G. 2014, ApJ, 788, 51

Papovich, C. et al. 2010, ApJ, 716, 1503

Pastrav B. A., Popescu C. C., Tuffs R. J., Sansom A. E., 2013, A& A, 557, A137

Peebles, P.J.E. 2001 ApJ, 557, 495

Poggianti, B. M. 1997, A& A, 122, 399

Popesso et al. 2005, A& A, 433, 415

Ryden, Barbara. *Introduction to Cosmology.* Ohio State Uni., 2007

Schechter P. 1976, ApJ, 203, 297

Spinrad H., 2005, Galaxy Formation and Evolution, Springer-Verlag, Berlin

Tovmassian, H. & Plionis, M., 2009, ApJ, 696, 1441

van der Wel A. et al., 2007, ApJ, 670, 206

van de Weygaert, R., Platen, E. 2011 IJMPS, 1, p. 4

Wen, Z. L. & Kan, J. L. 2014, arXiv:1412.6865

West, M.J. 1994, MNRAS, 268, 79

Wintraecken, J. *Large scale structure formation.* Retrieved from http://www.staff.science.uu.nl

Varvoglis, H & Seiradakis, J.H.,: *Introduction to modern Astronomy*, Thessaloniki: Gargatanis , 1994

# Appendices

## A The $\chi^2$ minimization procedure

The most common statistical method to identify how well a theoretical model describes the observed data, is the $\chi^2$ minimization procedure.

Suppose that we make a measurement $(x_i, y_i)$ of a quantity $y$ for a given $x_i$. The expected value for $y_i$ according to the theory would be $f(x_i)$ and the total error of the experimental measurement (due to uncertainties of the measurement, etc.) would be $\sigma$. The probability to make this measurement is [1]

$$P(x_i) = \frac{1}{\sigma_i \sqrt{2\pi}} \exp\left[-\frac{1}{2}\left(\frac{y_i - f(x_i)}{\sigma_i}\right)^2\right] \tag{A.1}$$

Now suppose that we make N measurements of this quantity that are independence of each other. The total probability of obtaining this entire set of these N data points is equal to the product of the probability of each data point (C. Laub, T. Kuhl), so

$$P_{tot} = \prod_{i=1}^{N} P(x_i) = \left[\prod_{i=1}^{N} \frac{1}{\sigma_i \sqrt{2\pi}}\right] \exp\left[-\frac{1}{2}\sum_{i=1}^{N}\left(\frac{y_i - f(x_i)}{\sigma_i}\right)^2\right] \tag{A.2}$$

If we want to find the maximum probability we have to minimize the sum in the exponential term of $P_{tot}$, so, we define this quantity as

$$\chi^2 = \sum_{i=1}^{N}\left(\frac{y_i - f(x_i)}{\sigma_i}\right)^2 \tag{A.3}$$

and for $\chi^2_{min}$ we have the maximum probability. Thus, if the theoretical function $f(x_i, \mathbf{p})$, depends on a set of parameters, which correspond to the elements of the vector $\mathbf{p}$, we can test for which values of these parameters we get the maximum probability.d

In our case, $y_i$ is the number of galaxies in each bin in the magnitude distribution histogram, with the center of each bin being $M_i$. Furthermore, $f(x_i)$ is the theoretically expected number

[1] Probabilities are normalized to their maximum values (Plionis et al. 2011)

of galaxies $\Phi(M) \times V$ for the same central magnitude $M_i$, with $\mathbf{p} \equiv (\alpha, M^*, \phi^*)$, for instance. So, we have

$$\chi^2 = \sum_{i=1}^{N} \left( \frac{\Phi(M_i, \mathbf{p}) \times V - N_i}{\sqrt{N_i}} \right)^2 \tag{A.4}$$

where $N_i$ is the number of galaxies in each bin of the histogram and V the volume of the cluster's region.

For the best-fit parameters $\mathbf{p_0}$ we obtain the minimum $\chi^2_{min}$. When the parameters differ from these values, $\mathbf{p} \neq \mathbf{p_0}$, then $\chi^2$ increases, so $\Delta\chi^2 = \chi^2 - \chi^2_{min} > 0$. Limits of $\Delta\chi^2$ that depend on the number of the fitted parameters, $N_f$, define confidence regions that contain a certain fraction of the probability distribution of $\mathbf{p}$'s [1]. Almost every possibility region corresponds to a certain standard deviation $\sigma$. All these are shown in Table 9.

**Table 9:** $\Delta\chi^2$ limits for $N_f$ fitted parameters and different confidence levels.

| $\sigma$ | $P$ | $N_f = 1$ | $N_f = 2$ | $N_f = 3$ |
|---|---|---|---|---|
| $1\sigma$ | 68.3% | 1 | 2.3 | 3.53 |
| | 90% | 2.71 | 4.61 | 6.25 |
| $2\sigma$ | 95.4% | 4 | 6.17 | 8.02 |
| $3\sigma$ | 99.73% | 9 | 11.83 | 14.2 |

In order to see how good our fit is, we have to divide the minimum $\chi^2_{min}$ by the degrees of freedom, $d.o.f.$ and obtain the reduced chi-square, $\chi^2_{min}/d.o.f.$ If we have $N$ bins and $N_f$ fitted parameters, then $d.o.f. = N - N_f$. For a satisfactory fit we want $\chi^2_{min}/d.o.f. \leq 1$, which implies that our model describes the observational data very well, inside our uncertainties limits. If $\chi^2_{min}/d.o.f. \gg 1$ it means that our model is not an appropriate fitting function or that we have not taken into account some form of unknown systematic error. Finally, we may have underestimated our observational uncertainties (Bremer, 2009).

[1] For more information see "Numerical Recipes 3rd Edition: The Art of Scientific Computing", William H. Press

# B $\Phi(L)$ within $R = 1.5h_{72}^{-1}$ Mpc, in the g, i bands

In this appendix we present the absolute magnitude histograms and the fitted LFs for the whole sample of galaxies and separately for the ellipticals, spirals and irregulars, in the g and i bands.

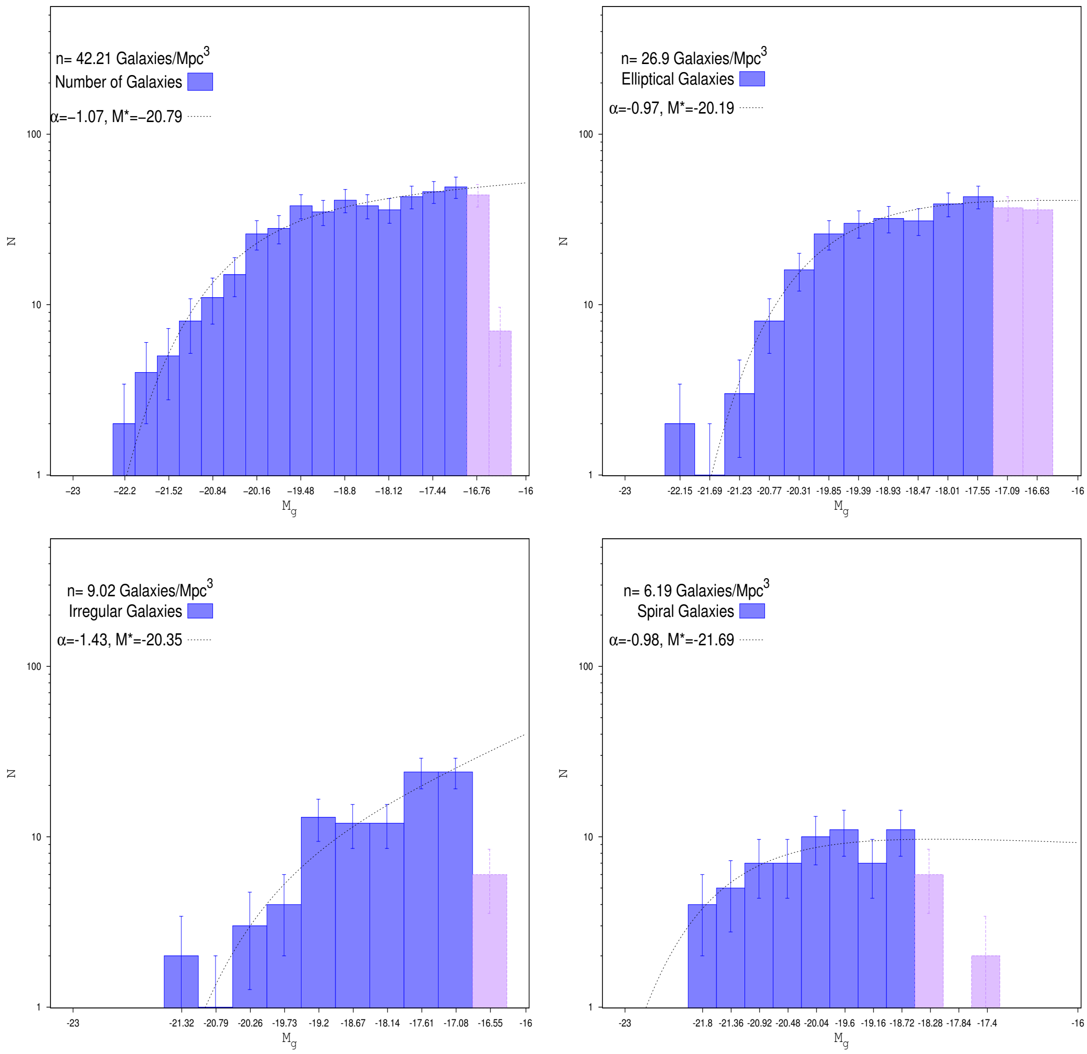


**Figure 13:** Galaxy luminosity functions in the g-band, for a radius $R = 1.5h_{72}^{-1}$ Mpc. *Left upper panel*: the whole sample of galaxies. *Right upper panel*: elliptical galaxies. *Left bottom panel*: irregular galaxies. *Right bottom panel*: spiral galaxies. The purple bins are those that have been eliminated from the analysis.

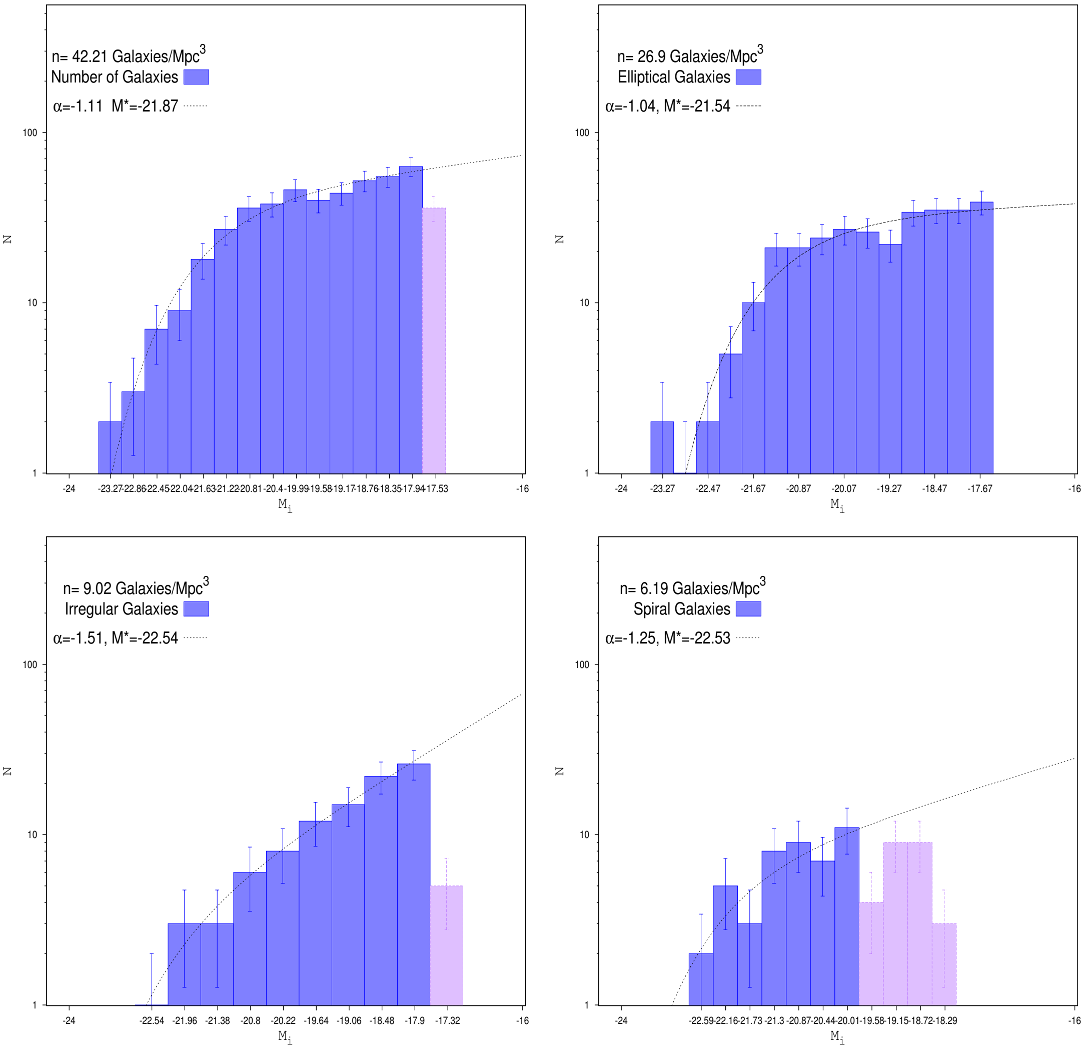


**Figure 14:** Galaxy luminosity functions in the i-band, for a radius $R = 1.5h_{72}^{-1}$ Mpc. *Left upper panel*: the whole sample of galaxies. *Right upper panel*: elliptical galaxies. *Left bottom panel*: irregular galaxies. *Right bottom panel*: spiral galaxies. The purple bins are those that have been eliminated from the analysis.

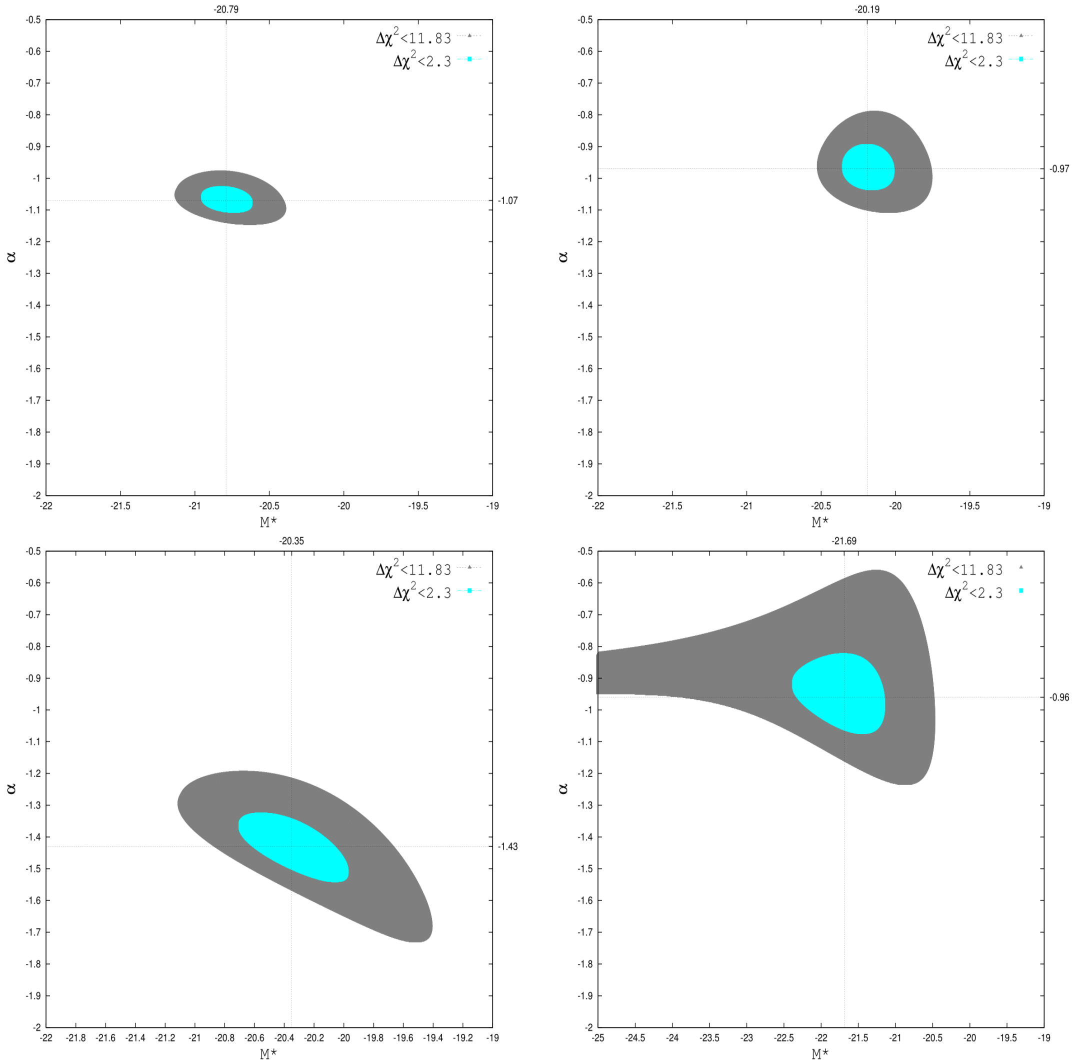


**Figure 15:** Solution space for $\alpha$ and $M^*$, in the g-band, for a radius $R = 1.5h_{72}^{-1}$ Mpc. The blue contour corresponds to the $1\sigma$ confidence level (68.3%) and the grey to the $3\sigma$ confidence level (99.73%). The best-fit values are at the intersections of the dashed lines. *Left upper panel*: the whole sample of galaxies. *Right upper panel*: elliptical galaxies. *Left bottom panel*: irregular galaxies. *Right bottom panel*: spiral galaxies.

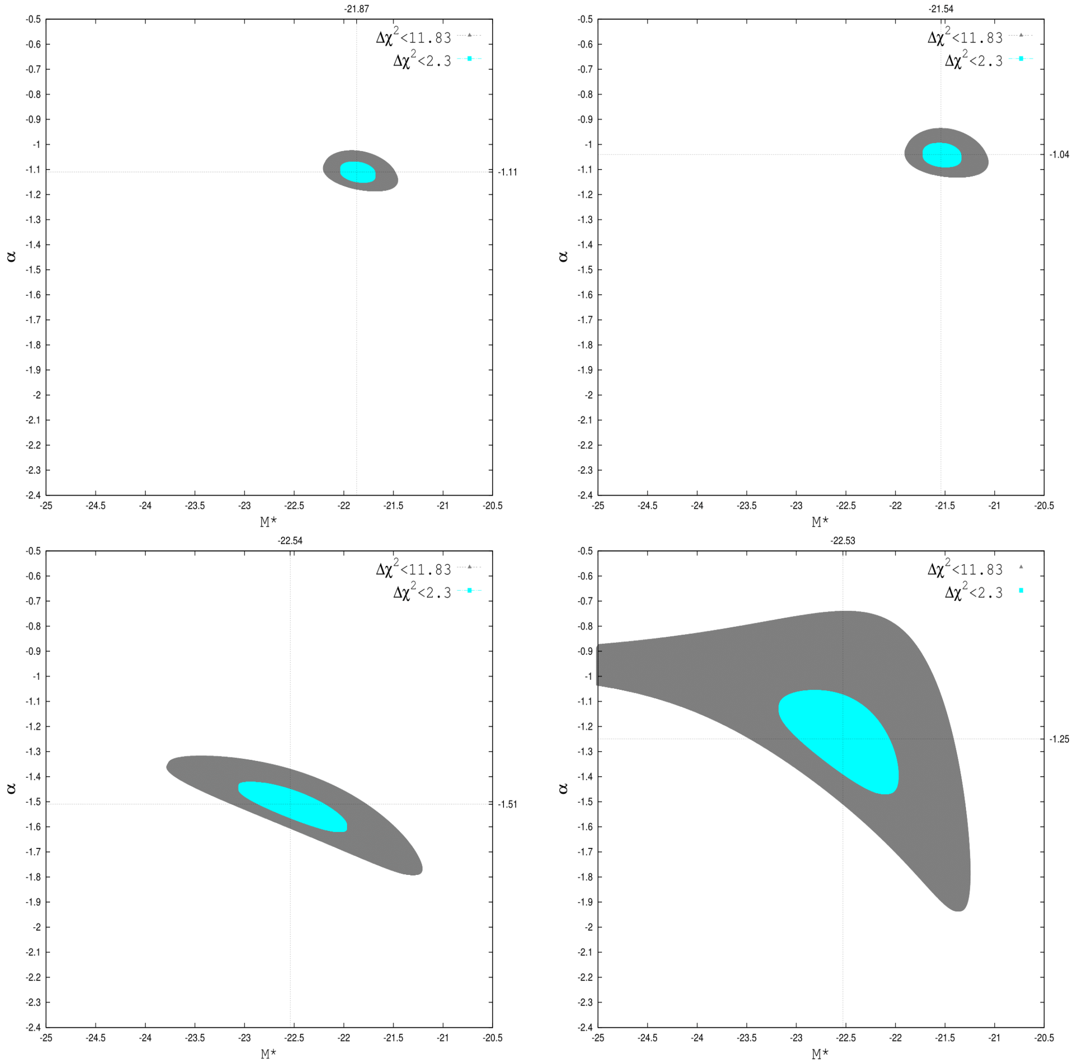


**Figure 16:** Solution space for $\alpha$ and $M^*$, in the i-band, for a radius $R = 1.5h_{72}^{-1}$ Mpc. The blue contour corresponds to the $1\sigma$ confidence level (68.3%) and the grey to the $3\sigma$ confidence level (99.73%). The best-fit values are at the intersections of the dashed lines. *Left upper panel*: the whole sample of galaxies. *Right upper panel*: elliptical galaxies. *Left bottom panel*: irregular galaxies. *Right bottom panel*: spiral galaxies.

## C $\Phi(L)$ of the core & the cluster outskirts, in the g, i bands

In this appendix we present the absolute magnitude histograms and the fitted LFs for the whole sample of galaxies and for the three types of galaxies separately (in the g and i band) and for the three selected regions $R = 1h_{72}^{-1}$ Mpc, $1h_{72}^{-1}$ Mpc $\leq R \leq 2.5h_{72}^{-1}$ Mpc and $1h^{-1}$ Mpc $\leq R \leq 1.75h^{-1}$ Mpc, respectively.

we also present

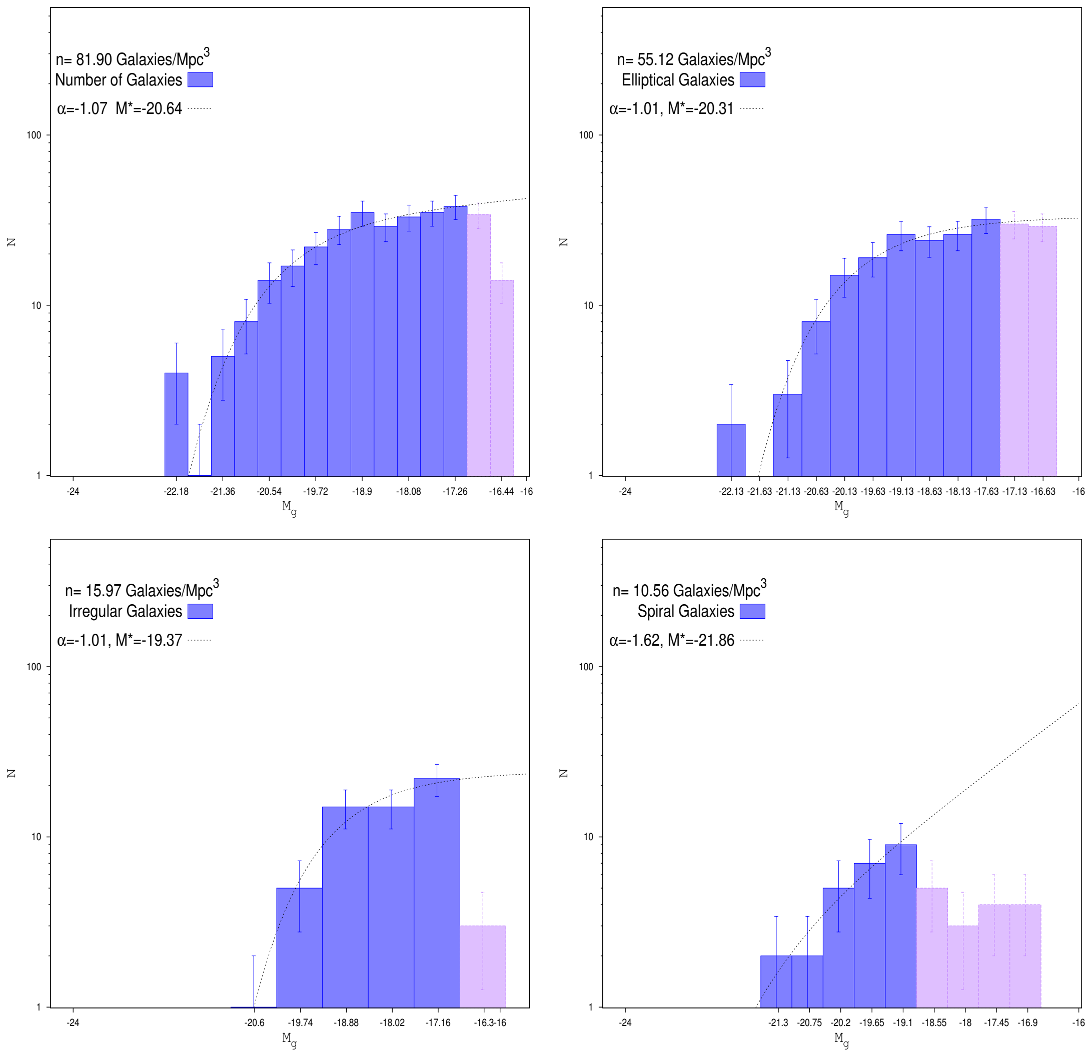


**Figure 17:** Galaxy luminosity functions of the cluster core, in the g-band, for a radius $R = 1h_{72}^{-1}$ Mpc. *Left upper panel*: the whole sample of galaxies. *Right upper panel*: elliptical galaxies. *Left bottom panel*: irregular galaxies. *Right bottom panel*: spiral galaxies. The purple bins are those that have been eliminated from the analysis.

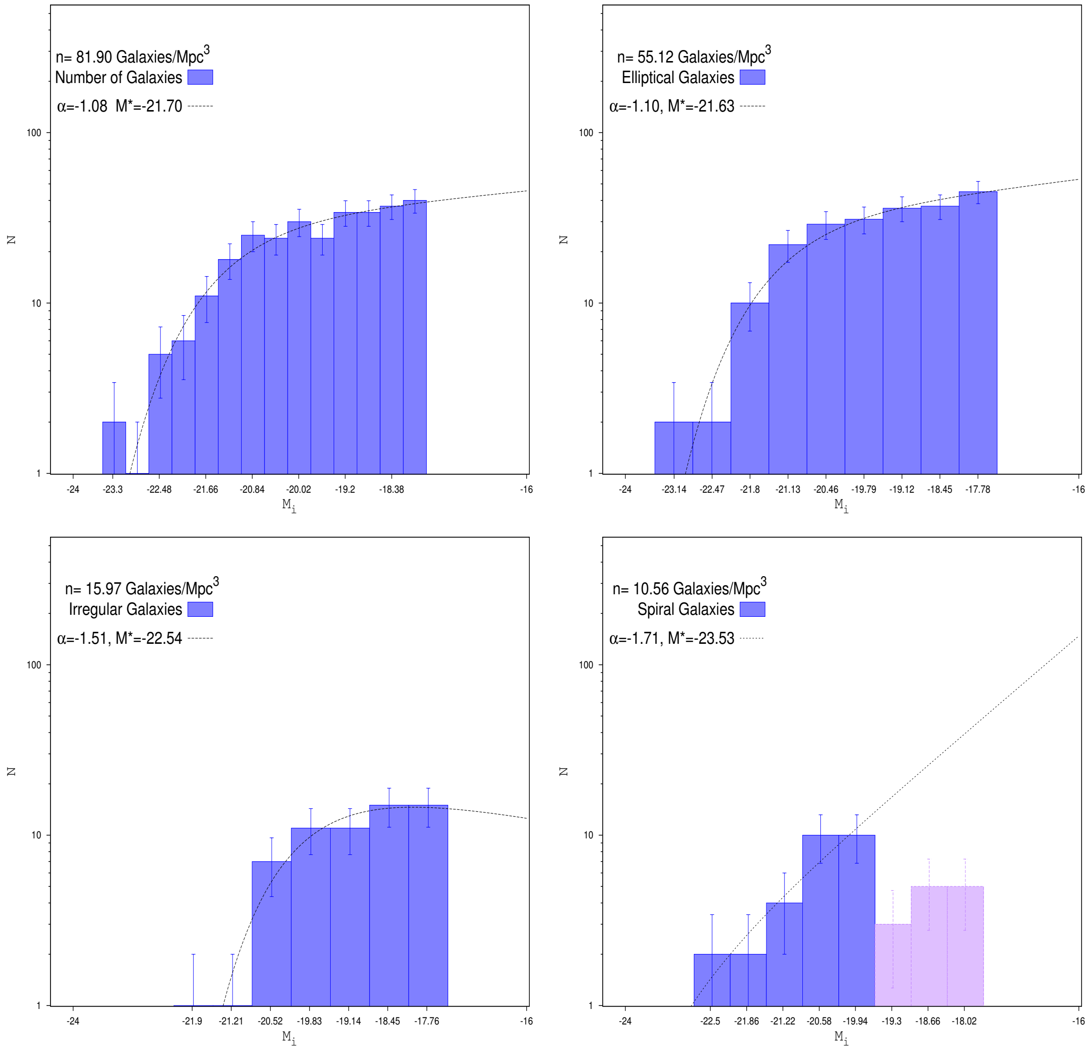


**Figure 18:** Galaxy luminosity functions of the clusterr core region, in the i-band, for a radius $R = 1h_{72}^{-1}$ Mpc. *Left upper panel*: the whole sample of galaxies. *Right upper panel*: elliptical galaxies. *Left bottom panel*: irregular galaxies. *Right bottom panel*: spiral galaxies. The purple bins are those that have been eliminated from the analysis.

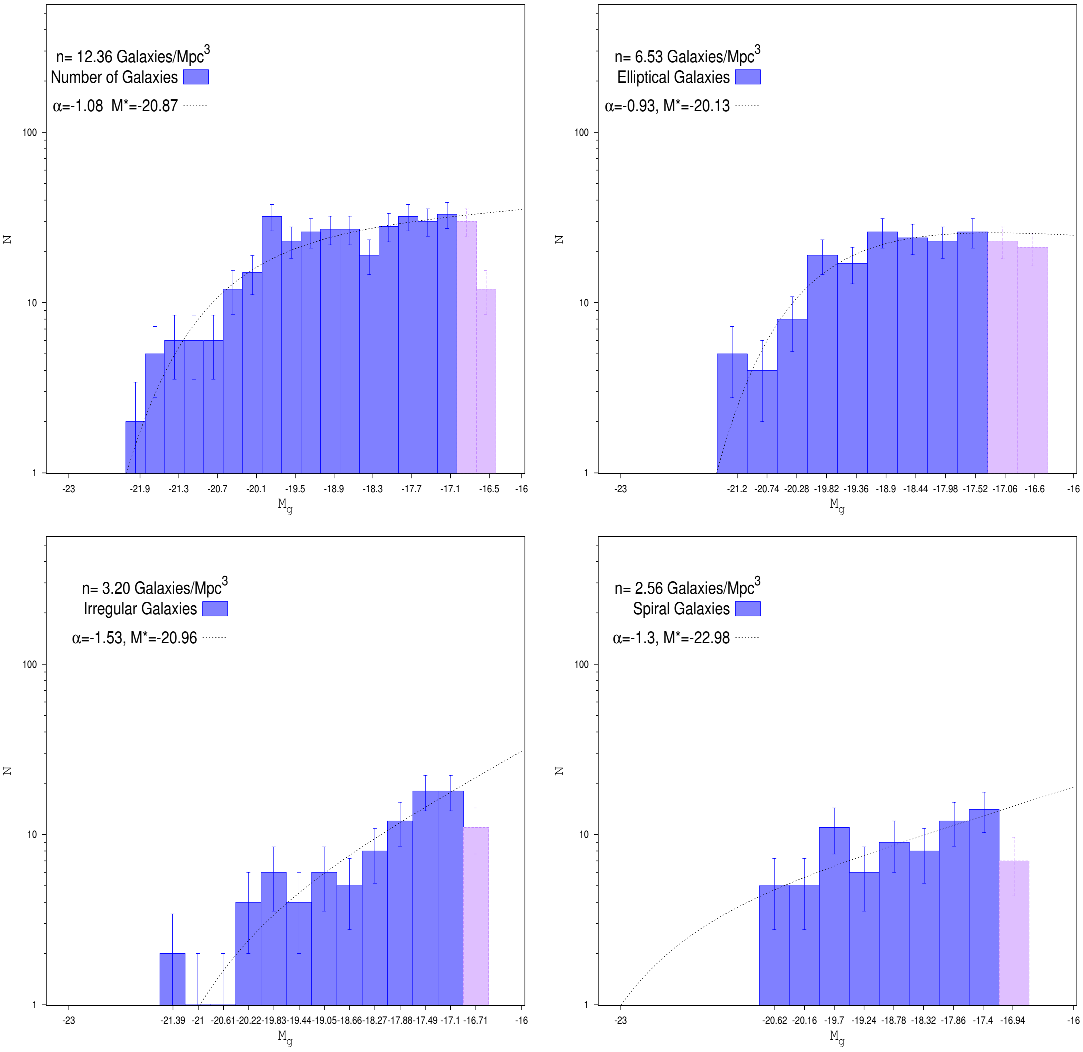


**Figure 19:** Galaxy luminosity functions, in the g-band, of the shell region: $1h_{72}^{-1}$ Mpc $\leq R \leq 2.5h_{72}^{-1}$ Mpc. *Left upper panel*: the whole sample of galaxies. *Right upper panel*: elliptical galaxies. *Left bottom panel*: irregular galaxies. *Right bottom panel*: spiral galaxies. The purple bins are those that have been eliminated from the analysis.

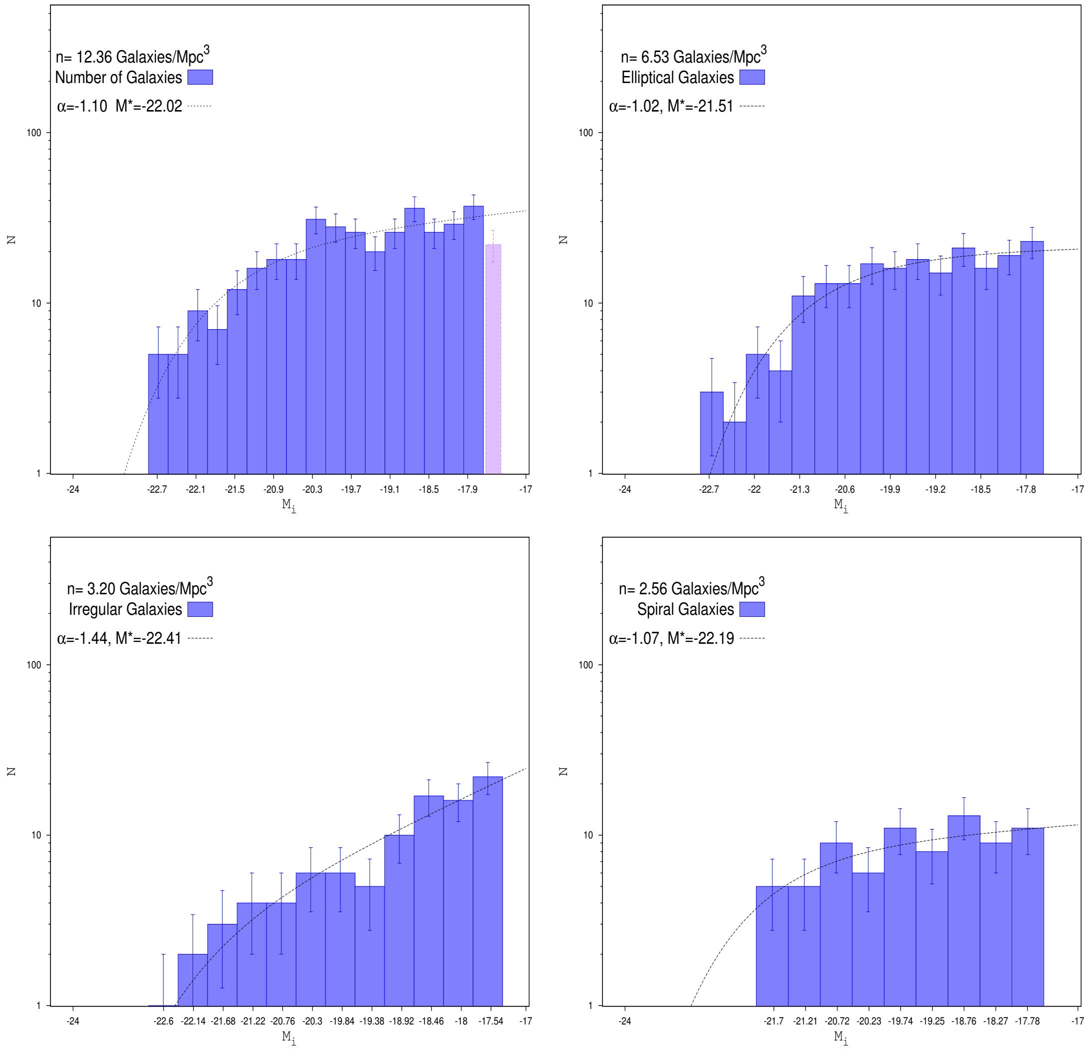


**Figure 20:** Galaxy luminosity functions, in the i-band, of the shell region: $1h_{72}^{-1}$ Mpc $\leq R \leq 2.5h_{72}^{-1}$ Mpc. *Left upper panel*: the whole sample of galaxies. *Right upper panel*: elliptical galaxies. *Left bottom panel*: irregular galaxies. *Right bottom panel*: spiral galaxies. The purple bins are those that have been eliminated from the analysis.

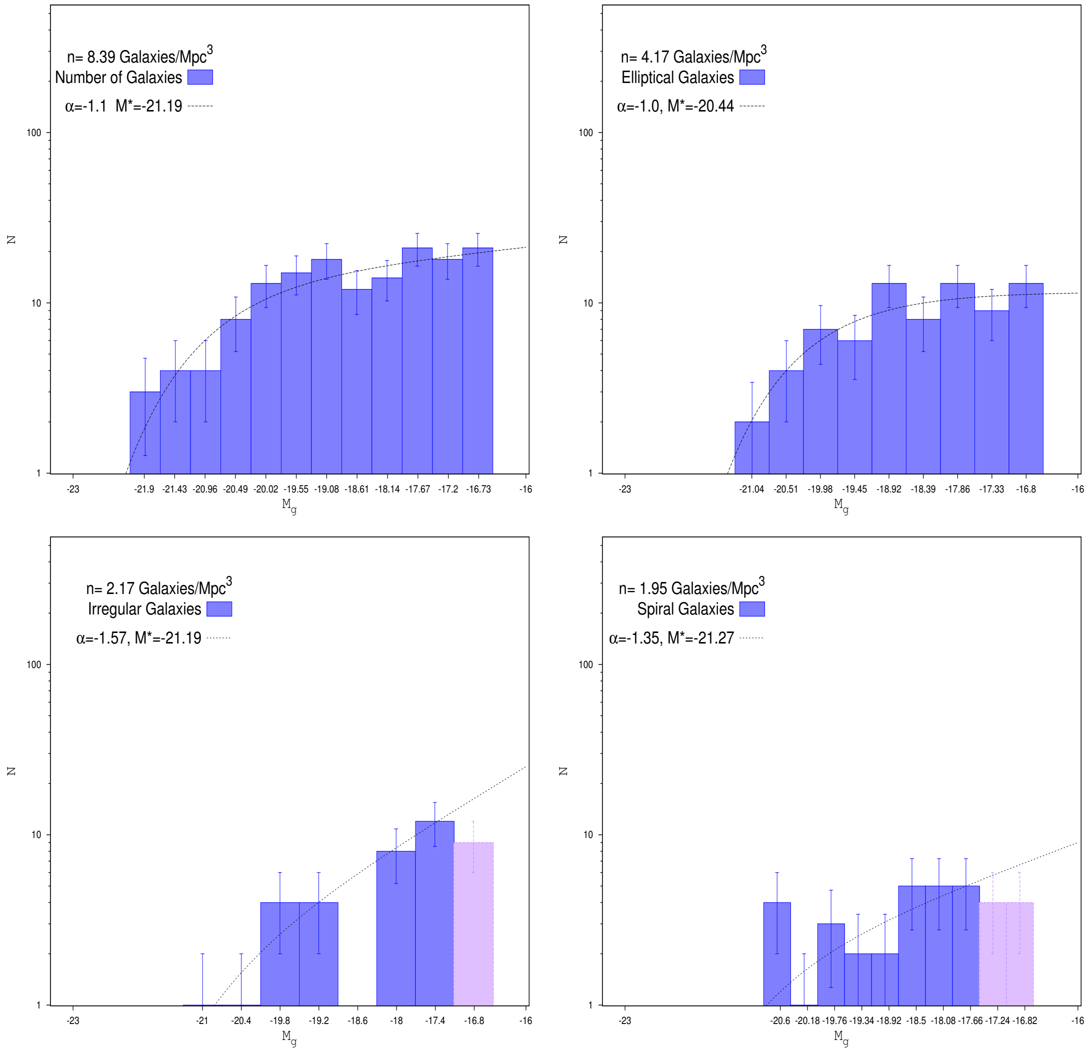


**Figure 21:** Galaxy luminosity functions, in the g-band, at cluster's shell region $1.75h_{72}^{-1}$ Mpc $\leq R \leq 2.5h_{72}^{-1}$ Mpc. *Left upper panel*: the whole sample of galaxies. *Right upper panel*: elliptical galaxies. *Left bottom panel*: irregular galaxies. *Right bottom panel*: spiral galaxies. The purple bins are those that have been eliminated from the analysis.

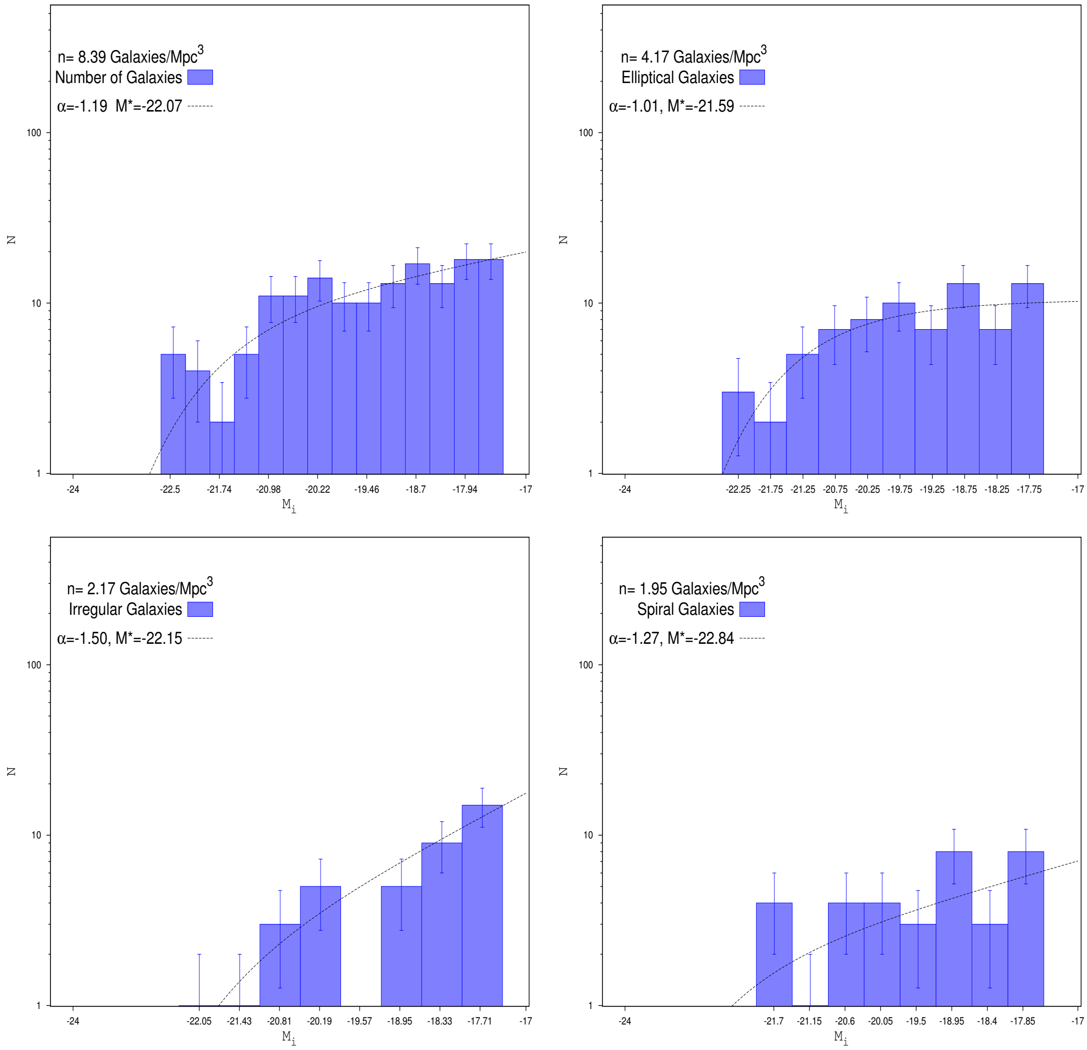


**Figure 22:** Galaxy luminosity functions, in the i-band, at cluster's shell region $1.75h_{72}^{-1}$ Mpc $\leq R \leq 2.5h_{72}^{-1}$ Mpc. *Left upper panel*: the whole sample of galaxies. *Right upper panel*: elliptical galaxies. *Left bottom panel*: irregular galaxies. *Right bottom panel*: spiral galaxies.

# D The dependence of the $\Phi(L)$ parameters on cluster-centric distance

In this appendix we present the best fit Schechter parameters in the three bands g, r, i, for the whole sample of galaxies and for the different type of galaxies separately in Table 10,Table 11, Table 12, at cluster's region $R = 0.5h_{72}^{-1}$ Mpc, $0.5h_{72}^{-1}$ Mpc $\leq R \leq 1h_{72}^{-1}$ Mpc, $1.75h_{72}^{-1}$ Mpc $\leq R \leq 2.5h_{72}^{-1}$ Mpc respectively.

We also present the diagrams of the dependence of the two Schechter parameters $\alpha$ and $M^*$ on the radial distnce from the cluster's center, in the g and i band.

**Table 10:** Best fit Schechter parameters in the three bands g, r, i, for the whole sample of galaxies and for the different types of galaxies separately, within a radius of $R = 0.5h_{72}^{-1}$ Mpc. The uncertainty of the parameters $\alpha$ and $M^*$, is the range for which $\Delta\chi^2 \leq 2.3$ when the parameter $\phi^*$ is fixed at its best value.

| Band | Type | $\alpha$ | $M^*$ | $\phi^*[h^3\ Mpc^{-3}]$ | $\chi^2/d.o.f$ |
|---|---|---|---|---|---|
| | All Galaxies | $-1.26^{+0.040}_{-0.034}$ | $-21.99^{+0.377}_{-0.358}$ | 8.70 | 0.65 |
| g | Ellipticals | $-1.25^{+0.063}_{-0.053}$ | $-20.92^{+0.338}_{-0.315}$ | 8.90 | 0.93 |
| | Irregulars | $-1.37^{+0.080}_{-0.055}$ | $-24.63^{+1.219}_{-0.869}$ | 0.40 | 0.28 |
| | Spirals | $-0.98^{+0.216}_{-0.131}$ | $-20.89^{+1.155}_{-2.471}$ | 3.90 | 0.10 |
| | All Galaxies | $-1.29^{+0.045}_{-0.039}$ | $-22.20^{+0.277}_{-0.251}$ | 8.90 | 0.64 |
| r | Ellipticals | $-1.22^{+0.053}_{-0.046}$ | $-21.76^{+0.347}_{-0.317}$ | 8.90 | 0.70 |
| | Irregulars | $-1.45^{+0.085}_{-0.059}$ | $-25.09^{+0.995}_{-0.706}$ | 0.50 | 0.33 |
| | Spirals | $-1.08^{+0.144}_{-0.091}$ | $-23.09^{+2.067}_{-3.700}$ | 2.10 | 0.48 |
| | All Galaxies | $-1.30^{+0.036}_{-0.032}$ | $-22.97^{+0.322}_{-0.296}$ | 8.90 | 0.80 |
| i | Ellipticals | $-1.28^{+0.053}_{-0.044}$ | $-22.87^{+0.400}_{-0.1365}$ | 8.90 | 0.79 |
| | Irregulars | $-1.54^{+0.118}_{-0.077}$ | $-25.15^{+1.005}_{-0.673}$ | 0.40 | 0.48 |
| | Spirals | $-1.07^{+0.103}_{-0.066}$ | $-25.16^{+3.354}_{-1.841}$ | 1.40 | 0.42 |

**Table 11:** Best fit Schechter parameters in the three bands g, r, i, for the whole sample of galaxies and for the different type of galaxies separately, at cluster's shell region $0.5h_{72}^{-1}$ Mpc $\leq R \leq 1h_{72}^{-1}$ Mpc. The uncertainty of the parameters $\alpha$ and $M^{*}$, is the range for which $\Delta\chi^2 \leq 2.3$ when the parameter $\phi^{*}$ is kept fixed at its best value.

| Band | Type | $\alpha$ | $M^{*}$ | $\phi^{*}[h^3\ Mpc^{-3}]$ | $\chi^2/d.o.f$ |
|---|---|---|---|---|---|
| g | All Galaxies | $-0.95^{+0.095}_{-0.078}$ | $-20.48^{+0.323}_{-0.283}$ | 7.10 | 1.27 |
| | Ellipticals | $-1.06^{+0.079}_{-0.065}$ | $-20.33^{+0.361}_{-0.329}$ | 6.30 | 0.09 |
| | Irregulars | $-0.85^{+0.222}_{-0.156}$ | $-19.25^{+0.572}_{-0.562}$ | 3.80 | 0.10 |
| | Spirals | $-1.95^{+0.155}_{-0.103}$ | $-22.82^{+0.485}_{-0.339}$ | 0.10 | 0.54 |
| r | All Galaxies | $-1.08^{+0.055}_{-0.048}$ | $-21.37^{+0.284}_{-0.253}$ | 5.10 | 0.28 |
| | Ellipticals | $-1.17^{+0.069}_{-0.058}$ | $-21.37^{+0.369}_{-0.342}$ | 4.60 | 0.03 |
| | Irregulars | $-1.42^{+0.096}_{-0.071}$ | $-22.02^{+0.656}_{-0.541}$ | 0.60 | 0.01 |
| | Spirals | $-2.49^{+0.263}_{-0.166}$ | $-22.29^{+0.340}_{-0.227}$ | 0.10 | 1.11 |
| i | All Galaxies | $-1.07^{+0.061}_{-0.051}$ | $-21.44^{+0.273}_{-0.243}$ | 5.40 | 0.74 |
| | Ellipticals | $-1.06^{+0.079}_{-0.065}$ | $-21.42^{+0.351}_{-0.308}$ | 6.30 | 0.38 |
| | Irregulars | $-1.25^{+0.144}_{-0.105}$ | $-21.09^{+0.596}_{-0.550}$ | 1.60 | 2.30 |
| | Spirals | $-2.29^{+0.253}_{-0.148}$ | $-22.95^{+0.392}_{-0.264}$ | 0.10 | 1.03 |

**Table 12:** Best fit Schechter parameters in the three bands g, r, i, for the whole sample of galaxies and for the different type of galaxies separately, at cluster's shell region $1h_{72}^{-1}$ Mpc $\leq R \leq 1.75h_{72}^{-1}$ Mpc. The uncertainty of the parameters $\alpha$ and $M^{*}$, is the range for which $\Delta\chi^2 \leq 2.3$ when the parameter $\phi^{*}$ is kept fixed at its best value.

| Band | Type | $\alpha$ | $M^{*}$ | $\phi^{*}[h^3\ Mpc^{-3}]$ | $\chi^2/d.o.f$ |
|---|---|---|---|---|---|
| g | All Galaxies | $-1.02^{+0.059}_{-0.052}$ | $-20.71^{+0.237}_{-0.220}$ | 2.00 | 0.53 |
| | Ellipticals | $-0.91^{+0.137}_{-0.112}$ | $-19.97^{+0.283}_{-0.255}$ | 1.60 | 0.68 |
| | Irregulars | $-1.53^{+0.052}_{-0.042}$ | $-22.73^{+0.456}_{-0.361}$ | 0.10 | 0.41 |
| | Spirals | $-0.82^{+0.213}_{-0.152}$ | $-20.23^{+0.647}_{-0.952}$ | 1.20 | 0.94 |
| r | All Galaxies | $-1.01^{+0.047}_{-0.042}$ | $-21.35^{+0.244}_{-0.230}$ | 2.20 | 0.40 |
| | Ellipticals | $-0.94^{+0.078}_{-0.065}$ | $-20.87^{+0.301}_{-0.271}$ | 1.50 | 0.50 |
| | Irregulars | $-1.57^{+0.054}_{-0.043}$ | $-23.21^{+0.400}_{-0.332}$ | 0.10 | 0.22 |
| | Spirals | $-1.01^{+0.105}_{-0.079}$ | $-21.87^{+1.019}_{-2.927}$ | 0.60 | 0.40 |
| i | All Galaxies | $-1.02^{+0.046}_{-0.040}$ | $-21.73^{+0.246}_{-0.228}$ | 2.80 | 0.34 |
| | Ellipticals | $-0.97^{+0.074}_{-0.063}$ | $-21.36^{+0.293}_{-0.255}$ | 1.40 | 0.43 |
| | Irregulars | $-1.55^{+0.051}_{-0.041}$ | $-23.77^{+0.435}_{-0.361}$ | 0.10 | 0.29 |
| | Spirals | $-1.05^{+0.145}_{-0.102}$ | $-22.66^{+1.245}_{-2.817}$ | 0.50 | 0.905 |

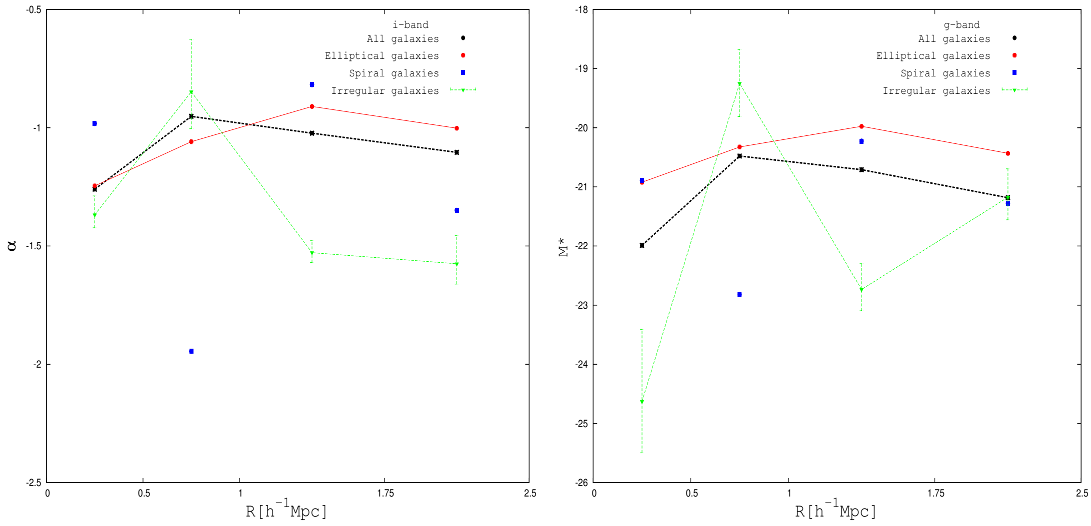


**Figure 23:** The dependence of the LF's parameters $\alpha$, $M^{*}$ on cluster-centric distance, in the g-band. *Left panel*: The dependence of $\alpha$ parameter on cluster-centric distance. *Right panel*: The dependence of $M^{*}$ parameter on cluster-centric distance.

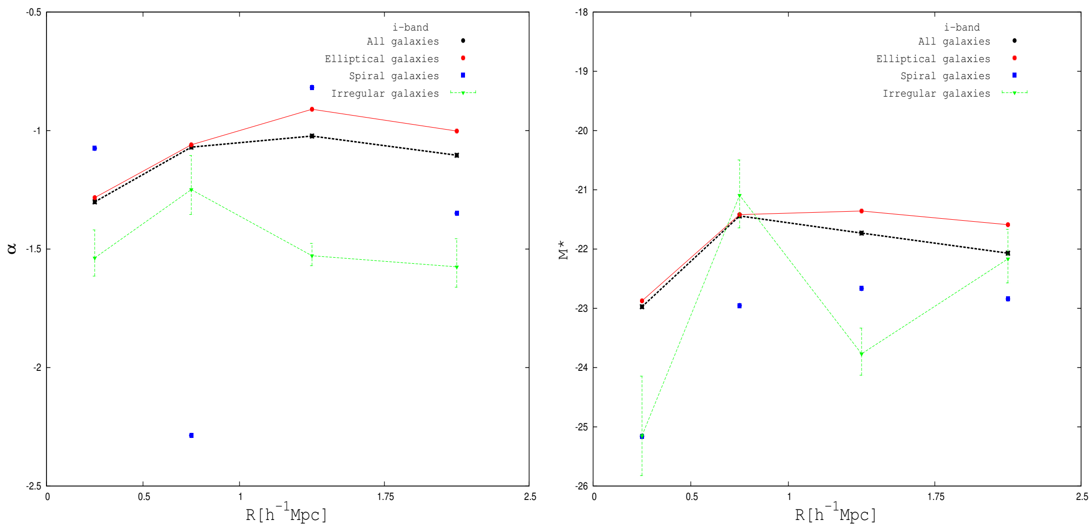


**Figure 24:** The dependence of the LF's parameters $\alpha$, $M^{*}$ on cluster-centric distance, in the i-band. *Left panel*: The dependence of $\alpha$ parameter on cluster-centric distance. *Right panel*: The dependence of $M^{*}$ parameter on cluster-centric distance.